INTERNATIONAL ATOMIC ENERGY AGENCY
UNITED NATIONS EDUCATIONAL, SCIENTIFIC AND CULTURAL ORGANIZATION
INTERNATIONAL CENTRE FOR THEORETICAL PHYSICS
I.C.T.P., P.O. BOX 586, 34100 TRIESTE, ITALY, CABLE: CENTRATOM TRIESTE

SMR.703 - 25

WORKING PARTY ON
MECHANICAL PROPERTIES OF INTERFACES

23 AUGUST - 3 SEPTEMBER 1993

"Dislocation-grainboundary Interactions in f.c.c. Materials"

"Basic Concepts and Models" Part I - (a) and (b)

J. DE HOSSON
University of Groningen
Department of Applied Physics
Nijenborgh 18
Groningen AG 9747
NETHERLANDS

These are preliminary lecture notes, intended only for distribution to participants.

PART-I-a

PHILOSOPHICAL MAGAZINE A, 1990, VOL. 61, NO. 2, 305–327

Atomic structure of (111) twist grain boundaries in f.c.c. metals

By J. TH. M. DE HOSSON and V. VITEK†

Department of Applied Physics, Materials Science Centre, University of Groningen, Nijenborgh 18, 9747 AG Groningen, The Netherlands

[*Received 9 January 1989‡ and accepted 5 May 1989*]

ABSTRACT

In this paper we have studied the atomic structures of (111) twist boundaries and investigated the applicability of the structural unit model which has previously been established for tilt boundaries and (001) twist boundaries by Sutton and Vitek. The calculations were carried out using two different descriptions of interatomic forces. A pair potential for aluminium, for which the calculations were made at constant volume, and a many-body potential for gold, for which the calculations were performed at constant pressure. The atomic structures of all the boundaries studied were found to be very similar for both the descriptions of atomic interactions. This suggests that the principal features of the structure of (111) twist boundaries found in this study are common to all f.c.c. metals. At the same time it supports the conclusion that calculations employing pair potentials are fully capable of revealing the generic features of the structure of grain boundaries in metals. The results obtained here, indeed, show that structures of all the boundaries with misorientations between 0° and 21·79° ($\Sigma=21$) are composed of units of the ideal lattice and/or the $\frac{1}{6}\langle 112\rangle$ stacking fault on (111) planes, and units of the $\Sigma=21$ boundary. Similarly, structures of boundaries with misorientations between 21·79° and 27·8° ($\Sigma=13$), 27·8° and 38·21° ($\Sigma=7$) and 38·21° and 60° ($\Sigma=3$) can all be regarded as decomposed into units of the corresponding delimiting boundaries. Therefore we conclude that the atomic structure of (111) twist boundaries can well be understood in the framework of the structural unit model. A related aspect analysed here in detail is the dislocation content of these boundaries. This study shows both the general relation between dislocation content and atomic structure of the boundaries, which is an integral part of the structural unit model, and features specific to the dislocation networks present in the (111) twist boundaries. Furthermore, the dislocation content revealed by the atomistic calculations can be compared in several cases with transmission electron microscope (TEM) observations and the results are discussed in this context.

§1. INTRODUCTION

Grain boundary phenomena usually take place in a very narrow region, of the order of a few atomic spacings, where the two grains meet. Hence understanding of the atomic structure of grain boundaries is a necessary precursor for the development of microscopic theories of boundary properties. For this reason the structure of grain boundaries has been investigated extensively in the last decade, both experimentally and with the help of computer simulations (see the proceedings of conferences edited by

† Permanent address: Department of Materials Science & Engineering, University of Pennsylvania, Philadelphia 19104, U.S.A.

‡ Received in final form 26 April 1989.

Rühle, Balluffi, Fischmeister and Sass (1985), Ishida (1986), Sass and Raj (1988) and Yoo, Briant and Clark (1988)). Such calculations contributed very significantly to our understanding of general features of grain boundary structure even though they were usually made using pair-potentials. While this is a crude approximation for most materials, significant results of these studies have often been found to be very little dependent on interatomic forces used and are common either to whole classes of materials or certain types of grain boundaries (for reviews see Balluffi (1982), Sutton (1984), Vitek and De Hosson (1986), Balluffi, Rühle and Sutton (1987) and De Hosson and Vitek (1987)).

One general result of this type is the structural unit model which relates structures of boundaries corresponding to different misorientations of the grains. The model was originally developed for periodic tilt boundaries (Sutton and Vitek 1983). It was later extended to (001) twist boundaries (Sutton 1982, Schwartz, Sutton and Vitek 1985, Schwartz, Bristowe and Vitek 1988) and recently it was generalized to non-periodic irrational tilt grain boundaries (Sutton 1988). In the case of (001) twist boundaries structures of all boundaries in a certain misorientation range are composed of mixtures of three different structural elements. They are the units of two short-period boundaries delimiting the misorientation range and certain 'filler' units. Structures of delimiting boundaries are contiguously composed of units of one type. Structure of a boundary with the misorientation in between two neighbouring delimiting boundaries can then be regarded as one of these delimiting boundaries with a superimposed rectangular network of screw displacement-shift-complete (DSC) dislocations related to the coincidence site lattice (CSL) of this delimiting boundary. The structure of the regions in between the dislocations is composed of units of this delimiting boundary while units of the other delimiting boundary are placed at the intersections of the dislocations. The rest of the cores of the DSC dislocations is composed of the filler units. The delimiting boundaries on the basis of which the whole misorientation range of (001) twist boundaries can be described correspond to $\Sigma=1$ (ideal crystal), $\Sigma=13$, 17 and 5 (Schwartz *et al.* 1985, Vitek 1988). These boundaries can be regarded as favoured boundaries according to the definition of Sutton and Vitek (1983). However, (001) twist boundaries are a rather special case. The purpose of the present paper is, therefore, to investigate the atomic structure of another class of twist boundaries with the aim of studying which structural features are common and which are specific to twist boundaries with different boundary planes. We concentrate here on the applicability of the structural unit model and demonstrate that the atomic structures of (111) twist boundaries can be well understood in this framework. A related aspect analysed here in detail is the dislocation content of these boundaries. This study shows both the general relation between dislocation content and atomic structure of the boundaries, which is an integral part of the structural unit model, and features specific to the dislocation networks present in the (111) twist boundaries. Furthermore, the dislocation content revealed by the atomistic calculations can be compared in several cases with transmission electron miscroscope (TEM) observations (Scott and Goodhew 1981, Hamelink and Schapink 1981, De Hosson, Schapink, Heringa and Hamelink 1986, Forwood and Clarebrough 1985, 1986) and the results are discussed in this context.

§2. General features of the dislocation content of (111) twist boundaries

The most important symmetry element governing structural features of (111) twist boundaries is the [111] threefold screw axis of the cubic lattice, which any dislocation

network present in these boundaries must possess. The results of atomistic studies, described in the following sections, show that such networks are either triangular or hexagonal. In general, such a network consists of three different types of dislocations with Burgers vectors $\mathbf{b}_i$ $(i=1,2,3)$ for which

$$\sum_i \mathbf{b}_i = 0. \tag{1}$$

The average separation, d, of dislocations in each set, is determined by Frank's formula (Frank 1950). Following Hirth and Lothe (1982), this condition can be expressed most conveniently by introducing the vectors

$$\mathbf{N}_i = N_i(\mathbf{n} \times \boldsymbol{\xi}_i), \tag{2}$$

where $\mathbf{n}$ is the unit vector in the direction of the boundary normal and $\boldsymbol{\xi}_i$ is the unit vector in the direction of the dislocations of type i.

$$N_i = 2d_i \sin\left(\frac{\Delta\Theta}{2}\right)^{-1} \tag{3}$$

where $\Delta\Theta$ is the misorientation across the boundary away from a reference state and d_i the average separation of dislocations of the set i. Owing to the threefold symmetry

$$\sum \mathbf{N}_i = 0, \tag{4}$$

and the magnitudes of all three vectors $\mathbf{N}_i$ are the same. Hence all the average separations d_i are also the same and in the following they are marked d. Noting that the rotation axis is in this case parallel to the boundary normal, Frank's formula reads

$$\mathbf{V} \times \mathbf{n} = \sum_i \mathbf{b}_i(\mathbf{N}_i \cdot \mathbf{V}), \tag{5}$$

where $\mathbf{V}$ is an arbitrary vector in the boundary plane.

Using conditions (1) and (4), eqn. (5) can be written as

$$\mathbf{V} \times \mathbf{n} = (2\mathbf{b}_1 + \mathbf{b}_2)(\mathbf{N}_1 \cdot \mathbf{V}) + (2\mathbf{b}_2 + \mathbf{b}_1)(\mathbf{N}_2 \cdot \mathbf{V}), \tag{6}$$

and since it has to be satisfied for any vector $\mathbf{V}$ it represents six linear equations for the components of the vectors $\mathbf{N}_1$ and $\mathbf{N}_2$. In the coordinate system for which the x axis is parallel to the boundary normal, $\mathbf{n}$, and the y axis is parallel to the projection of the Burgers vector $\mathbf{b}_1$ in the boundary plane, the solution is $\mathbf{N}_1 = (1/b)[0, -2/3, 0]$ and $\mathbf{N}_2 = (1/b)[0, -1/3, 1/\sqrt{3}]$, where b is the magnitude of the projection of the Burgers vectors of the dislocations to the boundary plane; owing to the threefold symmetry b is the same for all three types of dislocations. The Burgers vectors of these dislocations may have components perpendicular to the boundary but it follows from eqns. (1) and (6) that these components have to satisfy the conditions $b_2\perp = b_3\perp = -b_1\perp/2$. However, all the dislocations found in the present atomistic studies have Burgers vectors parallel to the boundary plane.

When the vectors $\mathbf{N}_1$ and $\mathbf{N}_2$ are known the average separation of the dislocations of the network can be found using eqn. (3). In the present case this gives

$$d = \frac{3b}{4\sin(\frac{1}{2}\Delta\Theta)}. \tag{7}$$

In the case of regular triangular networks this is directly the separation of the dislocations forming the sides of the triangles. In regular hexagonal networks dislocations forming a given set of parallel sides of the hexagons are effectively broken into segments the total length of which is equal to the one third of the length these dislocations would have if they were not segmented. Hence the separation of the dislocations forming a given set of the sides of the hexagons is equal to $d/3$.

When well localized dislocations can be identified in grain boundaries a significant elastic energy is associated with such a network. This was first recognized by Read and Shockley (1950), who evaluated this energy as a function of $\Delta\Theta$ for pure tilt boundaries and showed that it is responsible for the existence of cusps on a plot of the energy against misorientation dependence for misorientations corresponding to certain special boundaries which serve as reference structures for other grain boundaries. An exact evaluation of the elastic energy of a tilt boundary as the strain energy of a wall of edge dislocations is presented in Hirth and Lothe (1982) for the case of isotropic elasticity. Using the same method, the elastic energy of a rectangular network of screw dislocations, applicable to (001) twist boundaries, has recently been derived by Vitek (1987), and we present here a similar calculation for the network composed of three sets of screw dislocations, which is a good approximation for dislocation networks found in (111) twist boundaries.

To evaluate the elastic energy of a network of screw dislocations, we consider in a similar fashion to Hirth and Lothe (1982, p. 740), a pair of such networks of opposite sign formed in an infinite crystal. The specific energy of formation of such a pair, when well separated, is then twice the energy per unit area of the network. The average separation of the dislocations in this network given by Frank's formula, eqn. (7), is d, and owing to the threefold symmetry the average length of the dislocations separated by d is $l=2d/\sqrt{3}$. Let us take the plane of the boundary as the zy plane with one set of dislocations parallel to the z axis. The force in the direction x (perpendicular to the boundary) per unit length of a dislocation of opposite sign which lies parallel to the z axis is $-\sigma_{23}b$, where b is the magnitude of its Burgers vector and σ_{23} the corresponding component of the stress field associated with the network in the zy plane. The energy per length l per dislocation in one boundary can then be calculated as one half of the interaction energy of this dislocation with the dislocation network and is equal to

$$W=\frac{1}{2}\int_0^l\int_{r_0}^{\infty}\sigma_{23}\,b\,\mathrm{d}x\,\mathrm{d}z, \tag{8}$$

where r_0 is the core radius of the dislocations. The elastic energy per unit area of the boundary is then

$$\gamma_{el}=\frac{W}{S}=\frac{3\sqrt{3}}{2}\frac{W}{d^2}, \tag{9}$$

where $S=l^2/2\sqrt{3}=2d^2/3\sqrt{3}$ is the area per dislocation segment of length l.

In the framework of the linear isotropic elasticity the stress field associated with the dislocation network can be evaluated as a sum of the stresses of individual dislocations. Following the same procedure as employed in the case of the wall of edge dislocations

by Hirth and Lothe (1982, p. 731), we obtain for the network of three screw dislocations related by a threefold axis symmetry operation

$$\sigma_{23}=\frac{Gb}{2d}\left[\frac{2\sinh\left(\frac{2\pi x}{d}\right)}{\cosh\left(\frac{2\pi x}{d}\right)-\cos\left(\frac{2\pi y}{d}\right)}-\frac{\sinh\left(\frac{2\pi x}{d}\right)}{\cosh\left(\frac{2\pi x}{d}\right)-\cos\left(\frac{\pi(z\sqrt{3}+y)}{d}\right)}-\frac{\sinh\left(\frac{2\pi x}{d}\right)}{\cosh\left(\frac{2\pi x}{d}\right)-\cos\left(\frac{\pi(z\sqrt{3}-y)}{d}\right)}\right], \tag{10}$$

where G is the shear modulus. After inserting eqn. (10) into eqns. (8) and (9) (for $y=0$) and carrying out the integration as in Vitek (1987), we obtain

$$\gamma_{el}=\frac{Gb^2\sqrt{3}}{8\pi^2 d}\{\ln[\cosh\alpha+(\cosh\alpha^2-1)^{1/2}]-\ln(\cosh\alpha-1)-\ln 2\}, \tag{11}$$

where $\alpha=2\pi r_0/d$. For small misorientations, when $\Delta\Theta\ll 1$, $d\approx 3b/2\,\Delta\Theta\gg r_0$ and $\alpha\ll 1$, we can write $\cosh\alpha\approx 1+\alpha^2/2$. Equation (11) then gives, when neglecting in the curly brackets all the terms of order higher than α,

$$\gamma_{el}=\frac{Gb^2\sqrt{3}}{4\pi d}\left[\frac{\pi r_0}{d}-\ln\left(\frac{2\pi r_0}{d}\right)\right]. \tag{12}$$

Using the above expression for d we obtain

$$\gamma_{el}=\frac{Gb\sqrt{3}}{6\pi}\left[\frac{2\pi r_0}{3b}\Delta\Theta+\ln\left(\frac{3b}{4\pi r_0}\right)-\ln\Delta\Theta\right]\Delta\Theta \tag{13}$$

This formula is very similar to that obtained by Vitek (1987) for the square grid of screw dislocations. It should be noted that the term $(2\pi r_0/3b)\,\Delta\Theta$ inside the square brackets in eqn. (13) cannot be neglected with respect to other terms, in general, particularly when $b\ll r_0$; this is often the case for grain boundary dislocations whose Burgers vectors are usually smaller than the spacing of nearest neighbours, which is a lower limit for r_0. No such term exists in the same approximation when evaluating the energy of a wall of edge dislocations (Hirth and Lothe 1982, Vitek 1987).

The energy of the grain boundary is then

$$\gamma=\gamma_0+2E_c/b+\gamma_{el}, \tag{14}$$

where E_c is the core energy (per unit length) of the dislocation and γ_0 is the energy of the corresponding reference state. This leads to the energy against misorientation dependence with cusps at $\Delta\Theta=0$ (i.e. at misorientations corresponding to the favoured boundaries, which has indeed been found in the present study).

§3. Method of atomistic calculations and interatomic forces

The method of calculation was principally the same as in a number of previous studies and has been described in detail elsewhere (Vitek, Sutton, Smith and Pond 1980). A block consisting of the atomic coordinates of an unrelaxed f.c.c. bicrystal, containing the chosen coincidence boundary, is first constructed in the computer using

the basic geometrical rules of the CSL. The periodicity imposed by the CSL in the boundary plane is then maintained during the relaxation. A relaxed structure is found by minimizing the total internal energy with respect to all atomic positions *and* the relative displacements of the adjoining grains. During the relaxation, relative displacements of atomic layers parallel to the boundary are also permitted and thus the net relative translation of the two grains occurs automatically. The relaxation procedure was a standard gradient method.

Two different descriptions of atomic interactions were used in this paper. One is the pair potential for aluminium constructed by Dagens, Rasolt and Taylor (1975) on the basis of the pseudo-potential theory. It possesses long-range Friedel oscillations but it was shown that these oscillations can be damped (Duesberry, Jacucci and Taylor 1979, Pettifor and Ward 1984) and thus it is reasonable to limit the interactions to a small number of neighbours. In the present case the interaction extends up to the fourth-neighbour shell. Pair potentials are generally density-dependent and the total energy contains a large volume term which contributes the major part of the total energy. Nevertheless, structural features of those defects which do not involve large density and coordination variation, like grain boundaries in metals, can be successfully investigated with the use of pair potentials, but the calculations have to be carried out at constant volume. In the present study this has been ensured by not allowing any total displacement of the grains perpendicular to the boundary plane. However, the complete evaluation of the energy requires inclusion of the density-dependent term and for this reason we do not report here the boundary energies for aluminium.

The other description of interactions used in the present calculations was the many-body potential for gold constructed recently by Ackland, Tichy, Vitek and Finnis (1987) using the general concept introduced by Finnis and Sinclair (1984). In this framework the total energy of a system of N atoms is written as

$$E_{\text{tot}}=\frac{1}{2}\sum_{i,j=1}^{N} V(r_{ij})-\sum_{i}\left(\sum_{j}\phi(r_{ij})\right)^{1/2}, \tag{15}$$

where both V and ϕ are pair potentials fitted empirically to reproduce the equilibrium lattice parameter, elastic constants, cohesive energy and vacancy formation energy. The first term in eqn. (15) is the pair interaction which is repulsive at small separation of atoms while the second term is always attractive and replaces the above mentioned density-dependent term accompanying the pair potentials.

When using the many-body potentials the calculation can be done at constant pressure and the energy always fully evaluated. Hence all the calculations employing the many-body potential for gold were carried out at constant pressure, which means that an overall expansion was allowed, and the energies of the corresponding boundaries are reported. However, in all cases studied, the atomic structures found when using the pair potential for aluminium and the many-body potentials are very similar and for this reason we only show structures obtained in the pair-potential studies. For a more detailed discussion of the effect of interatomic potential on computed structures reference is made to Vitek and De Hosson (1986) and Wolf and Lutsko (1989).

§4. Atomic structure of grain boundaries

Owing to the threefold symmetry of the [111] axis and the twofold symmetry of the [110] axis which lies in the (111) plane, the misorientations for which different

Misorientations and energies of (111) twist boundaries (calculated using a many-body potential for gold).

θ	Σ	E(mJ m^{-2})
7·34	183	190·0
11·63	73	224·0
13·17	57	228·0
15·18	43	233·0
17·89	31	240·0
21·79	21	237·0
24·43	67	245·5
26·01	237	247·0
27·80	13	246·0
29·41	291	248·0
30·59	97	251·0
32·31	39	248·0
33·99	79	246·0
35·57	201	243·0
38·21	7	238·0
43·57	49	236·0
46·83	19	224·5
50·57	37	210·0
52·66	61	191·5
53·99	91	189·2
60·00	3	17·3

Fig. 1

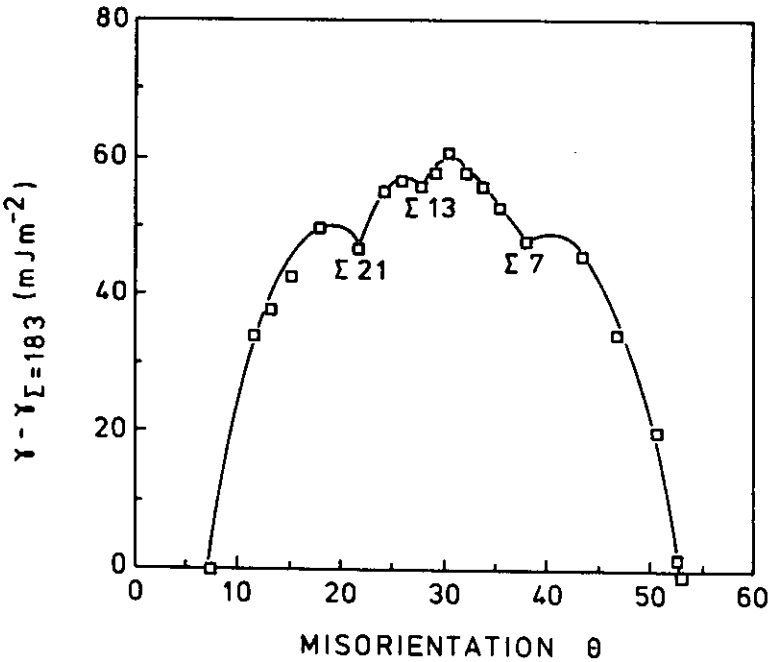

Energy against misorientation calculated using the many-body potential for gold. The squares represent values found in the atomistic calculations while the solid curve is an interpolation obtained when assuming the dependence of the type given by eqn. (14).

boundaries are found can be limited to the range 0° and 60°. In fact, it is the symmetry of the corresponding delimiting CSL boundaries ($\Sigma = 21, 13, 7$ and 3) which has to be taken into account, instead of the lattice symmetry. The corresponding CSLs have a third-order symmetry as well as a second-order one implied by the CSL 180° rotation axis (Bleris and Delavignette 1981, Doni, Bleris, Karakostas, Antonopoulos, Delavignette 1985). In this misorientation range we have simulated 21 different coincidence boundaries. Their reciprocal coincidence site densities, Σ, misorientation Θ, and energies found when using the many-body potential for gold, are summarized in the table. The dependence of grain boundary energy on misorientation is shown in fig. 1. Cusps are clearly visible at misorientations corresponding to $\Sigma = 21$, 13, 7 and 3, suggesting a special nature of these boundaries. The analysis of structures of these boundaries, presented below, indeed shows that for $0° < \Theta < 21{\cdot}79°$ they can be interpreted as composed of units of $\Sigma = 1$ and $\Sigma = 21$ boundaries; in the former case, units of the ideal crystal or the $\frac{1}{6}\langle 112\rangle(111)$ stacking fault occur in the boundary. For $21{\cdot}79° < \Theta < 27{\cdot}80°$ the boundary structures are composed of units of $\Sigma = 21$ and $\Sigma = 13$ boundaries, for $27{\cdot}80° < \Theta < 38{\cdot}21°$ of units of $\Sigma = 13$ and $\Sigma = 7$ boundaries, and for $38{\cdot}21° < \Theta < 60°$ of units of $\Sigma = 7$ and $\Sigma = 3$ boundaries. Hence, the short period boundaries corresponding to $\Sigma = 21, 13, 7$ and 3 are the favoured boundaries as defined by Sutton and Vitek (1983) and we first present their atomic structure and summarize possible related grain boundary dislocations.

4.1. *Structure of favoured boundaries*

The atomic structure of the $\Sigma = 21$ boundary is shown in fig. 2. In this and all the following figures the symbols △, +, □, * represent atoms in four different (111) planes adjacent to the boundary; the boundary plane is located between layers marked + and □. The fundamental structural unit of this boundary has the form of a hexagon and is delineated in fig. 2 by solid lines. The shortest DSC vectors related to this coincidence are of the type $(1/42)[\bar{5}41]$ and dislocations with this Burgers vector are associated with a step of height equal to the interplanar spacing of (111) planes (King 1982). On the other hand no steps are associated with the DSC dislocations having the Burgers vectors $(1/14)[\bar{3}21]$ or $(1/14)[\bar{5}41]$. All these dislocations have been identified in boundaries in the misorientation range $0° < \Theta < 21{\cdot}79°$.

The atomic structure of the $\Sigma = 13$ boundary is shown in fig. 3, where the basic structural unit is again delineated by solid lines. The shortest DSC vector corresponding to this coincidence is $(1/26)[\bar{4}31]$ and no steps are associated with these dislocations. Two possible atomic structures of the $\Sigma = 7$ boundary were found which differ in the relative displacement of the adjoining grains by $(1/28)[\bar{3}21]$; they are shown in figs. 4(*a*) and (*b*) respectively. The shortest DSC vectors ascribed to this coincidence are of the type $(1/14)[\bar{3}21]$ and no steps are associated with these dislocations. The structure shown in fig. 4(*a*) possesses a somewhat lower energy and is found in boundaries containing units of the $\Sigma = 7$ boundary.

The $\Sigma = 3$ boundary, which is the usual twin boundary in f.c.c. crystals, is also a favoured boundary. It is not shown here for reason of space, since its structure is commonly known, but units of this boundary are seen in fig. 11. The shortest DSC vector corresponding to this coincidence is $\frac{1}{6}[\bar{2}11]$. Dislocations with this Burgers vector are associated with a step of height one interplanar spacing of (111) planes.

Fig. 2

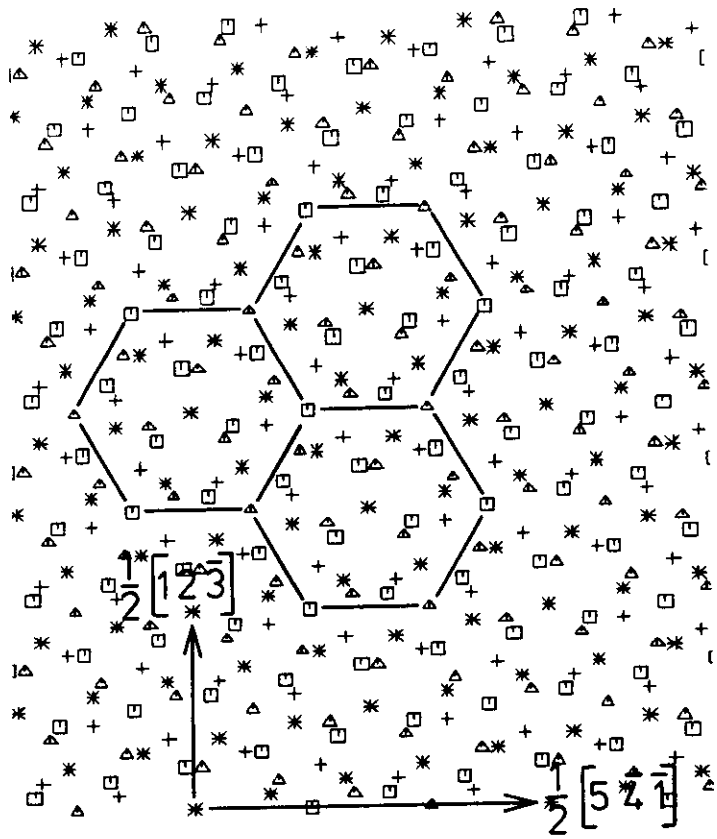

Structure of the $\Sigma = 21$ boundary.

4.2. *Low-angle boundaries* $0° < \Theta < 21{\cdot}78°$

A typical example of a low-angle grain boundary is that for $\Sigma = 183 (\Theta = 7{\cdot}34°)$. Its decomposition into the structural units which corresponds to decomposing the shortest CSL vector according to

$$\tfrac{1}{2}[5\bar{9}4] \rightarrow \tfrac{1}{2}[2\bar{3}1] + 9\tfrac{1}{6}[1\bar{2}1] \tag{15}$$

is depicted in fig. 5. The hexagons are clearly the units of the $\Sigma = 21$ boundary. The regions connecting $\Sigma = 21$ units correspond to the cores of grain boundary dislocations which intersect at the minority $\Sigma = 21$ units, in a similar manner to the case of (001) twist boundaries (Schwartz *et al.* 1985). As shown below, these dislocations appear to be the three partial dislocations of the type $\frac{1}{6}\langle 112\rangle$ lying in screw orientations. The triangular regions between these dislocations are then, alternatively, the ideal crystal and the stacking fault. The Burgers vectors of the three intersecting partials are: $\mathbf{b}_1 = \frac{1}{6}[11\bar{2}]$, $\mathbf{b}_2 = \frac{1}{6}[1\bar{2}1]$ and $\mathbf{b}_3 = \frac{1}{6}[\bar{2}11]$. Taking the ideal crystal as the reference structure, the average separation of the dislocations of the same type in the network is, according to Frank's formula (eqn. (7)), $d = 4{\cdot}782 a_0$, where a_0 is the lattice parameter. It is seen from

Fig. 3

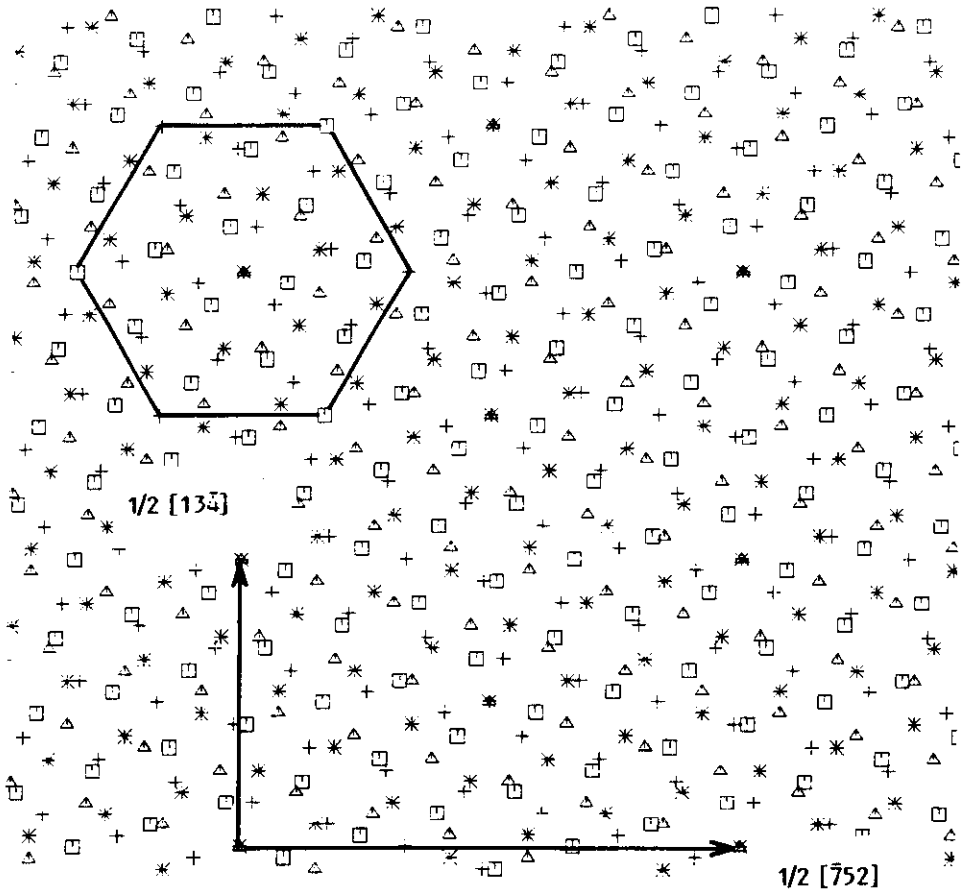

Structure of the $\Sigma = 13$ boundary.

fig. 5 that the separation of the dislocations is $|\frac{1}{4}[14\,\overline{13}\,\bar{1}]| = 4{\cdot}782a_0$, in agreement with Frank's rule.

For the $\Sigma = 57$ boundary, where the ratio of ideal crystal units and $\Sigma = 21$ units is 1 : 1, the situation is very similar to the case of $\Sigma = 183$ when considering the ideal crystal (together with the stacking fault) as a reference structure. The separation of the $\frac{1}{6}\langle 112\rangle$ dislocations is now $|\frac{1}{4}[\bar{8}71]| = 2{\cdot}669a_0$, in agreement with Frank's formula for $\Delta\theta = 13{\cdot}7°$. However, at this point the $\Sigma = 21$ boundary can also be regarded as the reference structure and the dislocation content expressed in terms of the DSC dislocations related to this coincidence, as described below for boundaries with misorientations larger than that of $\Sigma = 57$.

When moving to angles larger than 13·17°, units of the $\Sigma = 21$ boundary are in the majority and the ideal crystal and/or stacking fault act as intersections of the corresponding DSC dislocations preserving the $\Sigma = 21$ structure. An example is the $\Sigma = 43$ boundary shown in fig. 6(*a*). The corresponding network of grain boundary dislocations, shown schematically in fig. 6(*b*), is quite complex. It consists of screw

Fig. 4

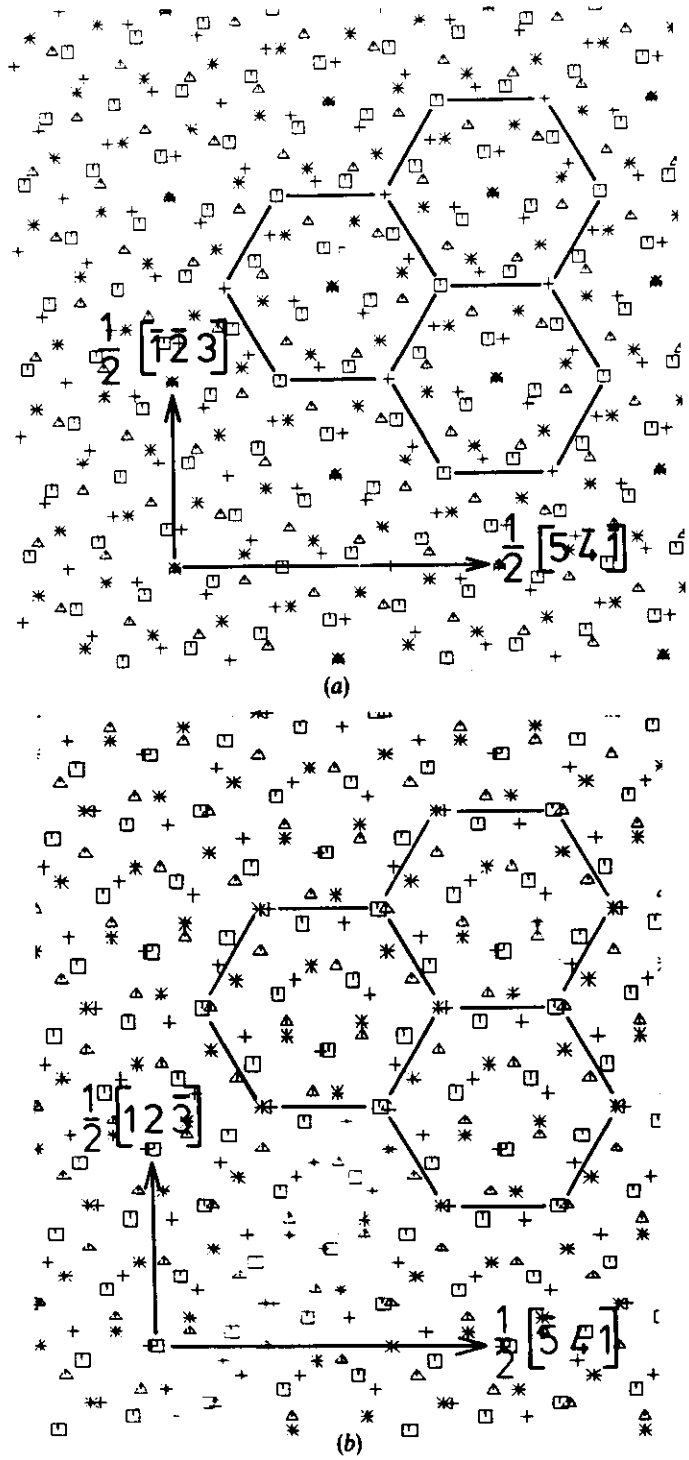

Two alternative structures of $\Sigma = 7$ which differ in the relative displacement of the adjoining grains by (1/28)[$\bar{3}$21]. The structure shown in (*a*) possesses a lower energy.

Fig. 5

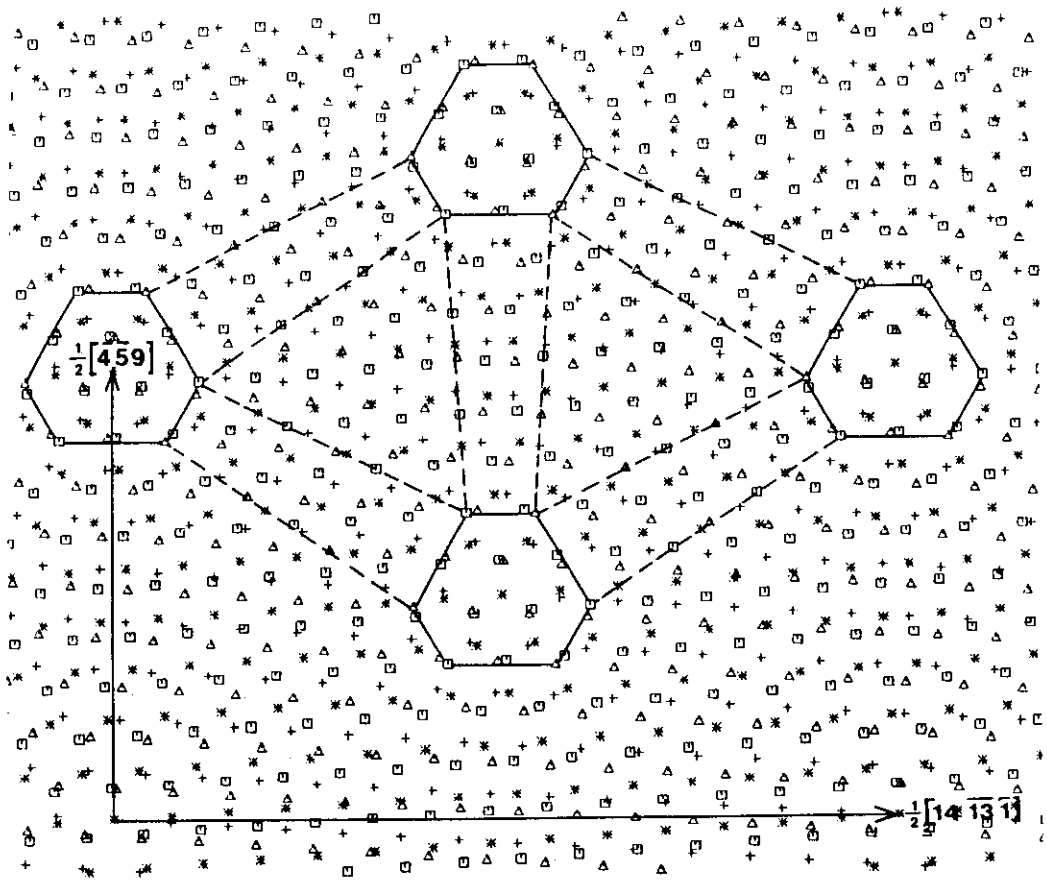

Structure of the $\Sigma = 183$ boundary: solid lines indicate $\Sigma = 21$ units whereas the dashed lines of Shockley partial dislocations form triangular regions.

dislocations of the type (1/14)[$\bar{5}41$] and edge dislocations of the type (1/14)[$\bar{3}21$]. These two types of dislocations are both DSC dislocations related to $\Sigma = 21$ but the latter do not contribute to the misorientation because of their edge character. The separation of the screw dislocations is found to be equal to $\frac{1}{4}|\frac{1}{2}[\bar{13}\,8\,5]| = 2{\cdot}008a_0$. Frank's formula based on (1/14)[$\bar{5}41$] and $\Delta\Theta = 6{\cdot}609°$ with respect to $\Sigma = 21$ would predict a separation of $6{\cdot}023a_0$. At first sight, this seems to be in conflict but one should notice that the dislocation network is hexagonal and, as explained in §2, the separation of the dislocations is then only one third of the average separation given by Frank's formula, which is in agreement with the separation determined from fig. 6(*a*).

4.3. *Misorientation range: 21·78° < Θ < 27·80°*

The structure for $\Sigma = 67$ ($\Delta\Theta = 2{\cdot}646$ with respect to $\Sigma = 21$) is presented in fig. 7. The grain boundary dislocations are the DSC dislocations of the type (1/42)[$\bar{5}41$]. Their separation is $|\frac{1}{4}[\bar{16}\,11\,5]| = 5{\cdot}012a_0$, which is in accordance with Frank's formula

Fig. 6

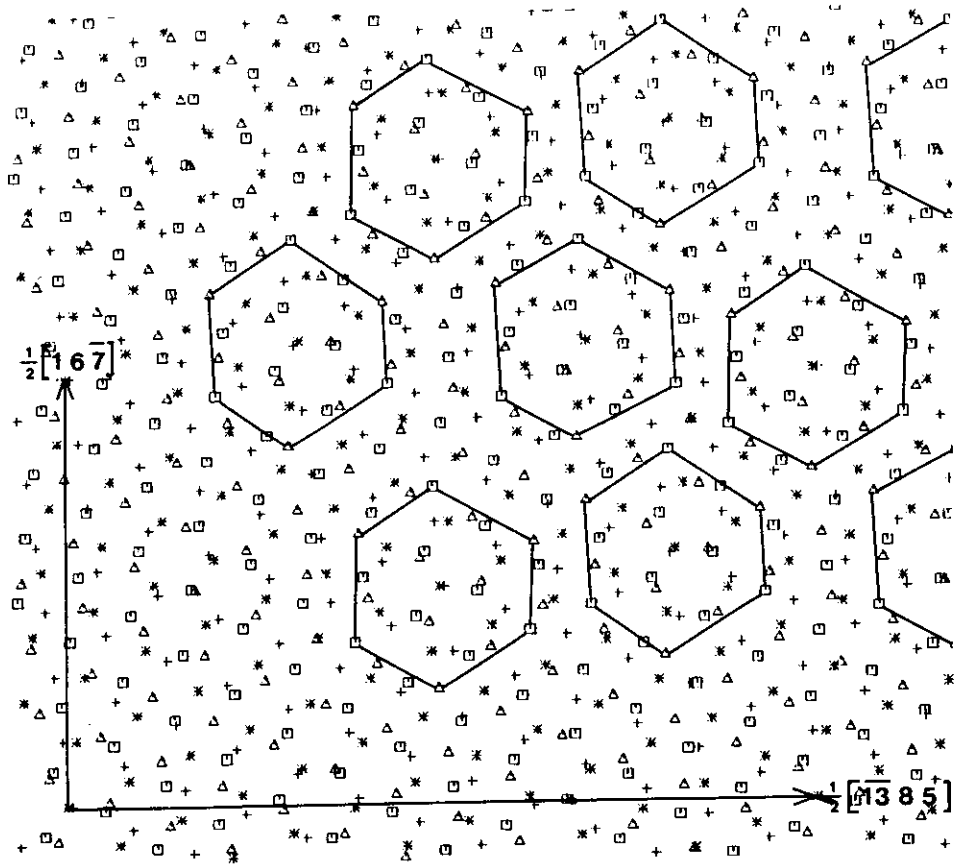

(a)

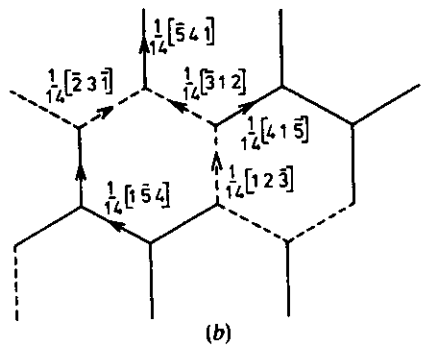

(b)

(a) Structure of the $\Sigma = 43$ boundary: solid lines indicate $\Sigma = 21$ units. (b) Schematic drawing of the corresponding network of grain boundary dislocations consisting of (1/14)[$\bar{3}$41] screw and (1/14)[$\bar{3}$21] edge components.

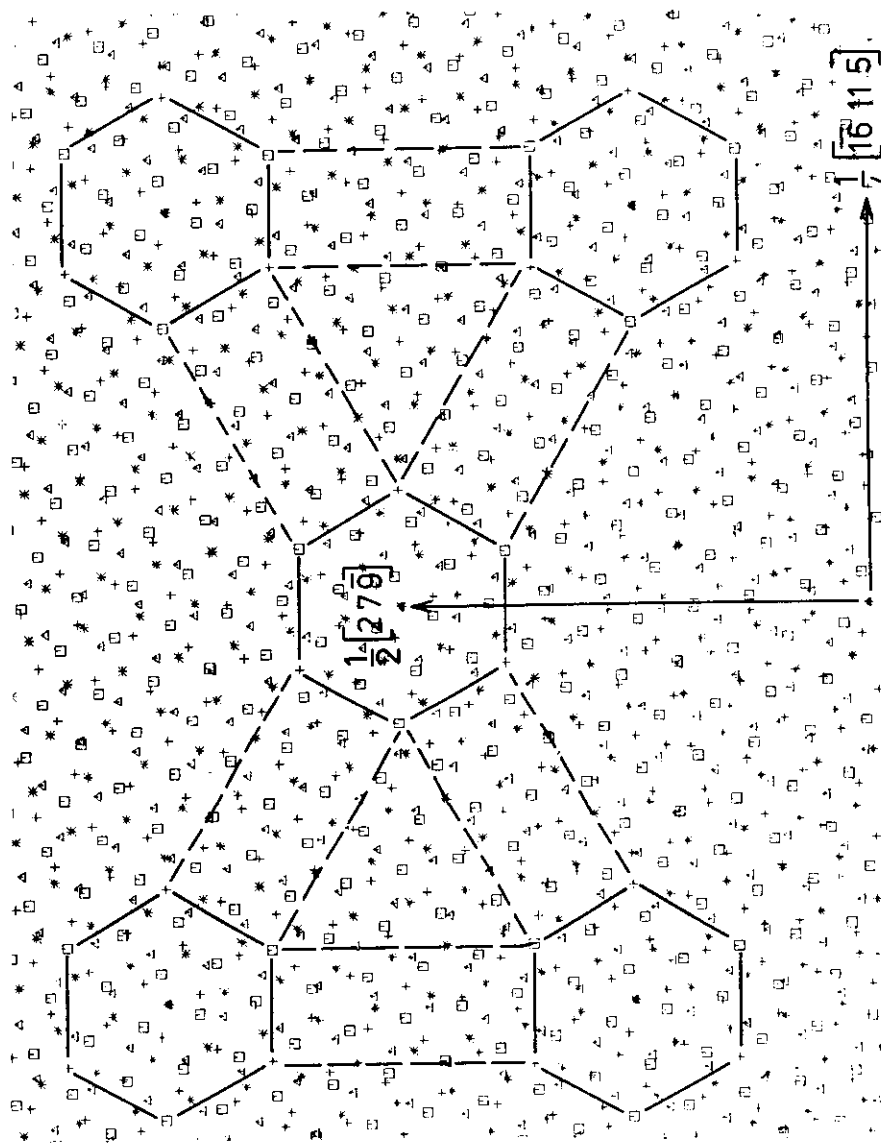

Fig. 7

Structure of the $\Sigma = 67$ boundary. $\Sigma = 13$ units are indicated by solid lines.

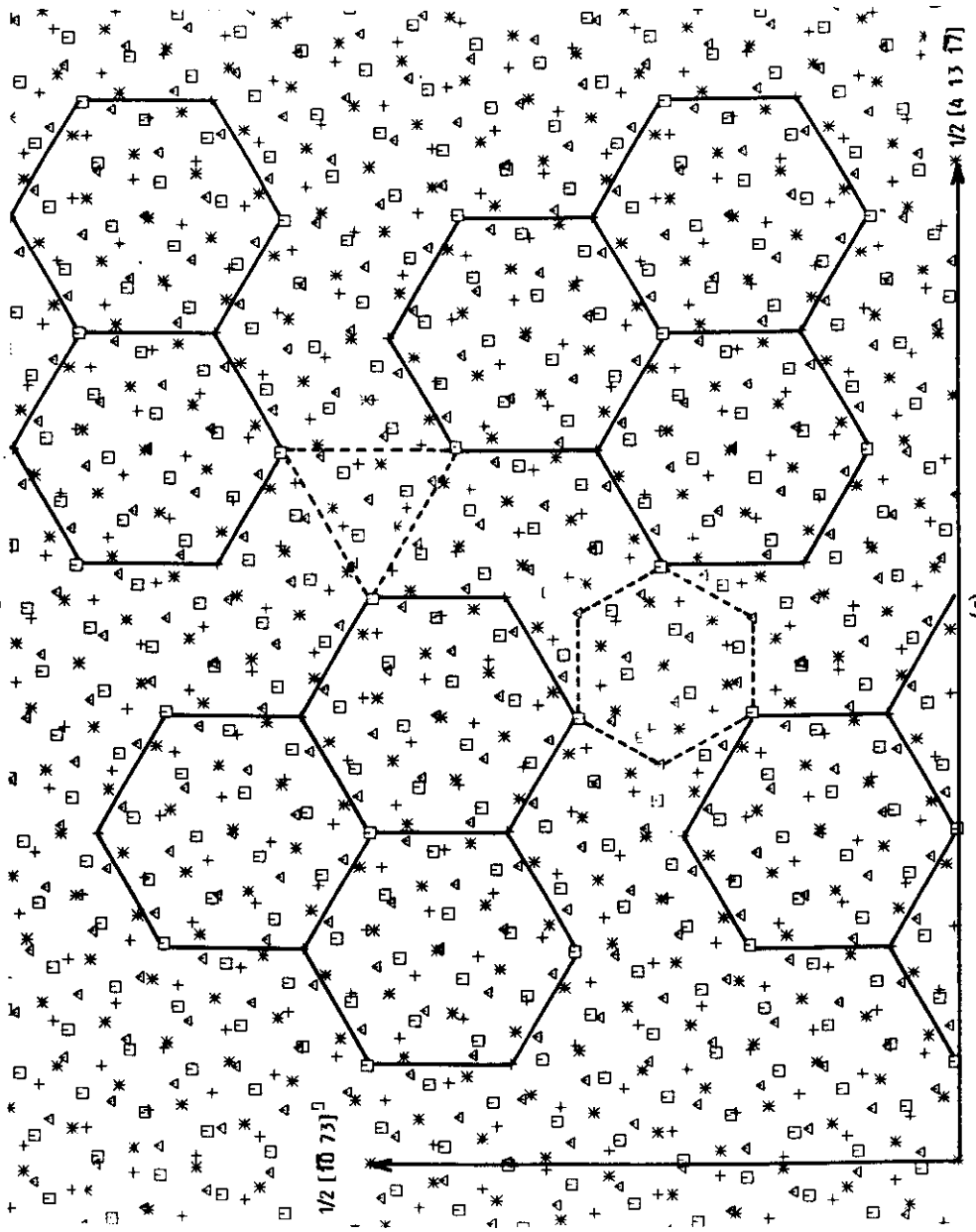

Fig. 8

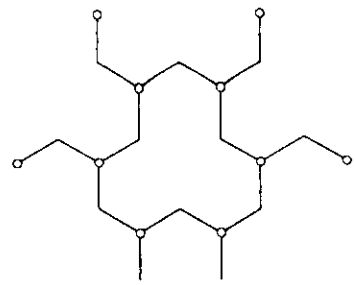

(b)

(a) Structure of the $\Sigma=237$ boundary: solid lines indicate $\Sigma=13$ units surrounded by DSC dislocations intersecting at $\Sigma=21$ units (dashed line). (b) Schematic drawing of grain boundary dislocations.

(eqn. (7)). The intersections of the dislocations are now units of the $\Sigma=13$ boundary and the dislocation network surrounds triangular areas of the $\Sigma=21$ structures which are alternately on different levels. The reason is that the DSC dislocations forming the network are associated with steps of height $\frac{1}{3}[111]$.

Figure 8(*a*) shows the structure of the $\Sigma=237$ boundary. The regions of the boundary, each composed of three hexagonal units of the $\Sigma=13$ boundary, are surrounded by DSC dislocations of the type $(1/26)[\bar{4}31]$, relating to the $\Sigma=13$ coincidence, which form the network shown schematically in fig. 8(*b*). These dislocations are not pure screw but each consists of two parts which have edge components of opposite sign. Their intersections are units and/or parts of the units of the $\Sigma=21$ boundary. It is seen from fig. 8(*a*) that the separation of the network dislocations with the same Burgers vector is $|\frac{1}{4}[\bar{1}0\,7\,3]|=3{\cdot}142a_0$. According to eqn. (7) we obtain $d=9{\cdot}427a_0$ for these DSC dislocations when taking the $\Sigma=13$ boundary as the reference structure; which means three times as much, in accordance with the fact that the network is hexagonal.

4.4. *Misorientation range* $27{\cdot}8° < \Theta < 38{\cdot}21°$

The structure of the $\Sigma=291$ boundary is shown in fig. 9. The composition of this boundary is analogous to that for $\Sigma=237$. The areas composed of three hexagonal units are again regions of the slightly distorted $\Sigma=13$ structure which are surrounded by DSC dislocations of the type $(1/26)[\bar{4}31]$. However, the dislocations intersect at regions corresponding to the $\Sigma=39$ boundary. The latter can, of course, be regarded as composed of 1 : 1 mixture of units of the $\Sigma=13$ and $\Sigma=7$ boundaries. The structure of the $\Sigma=79$, shown in fig. 10, is very similar, possessing the same regions of the $\Sigma=13$ boundary and the same dislocation network but the $(1/26)[\bar{4}31]$ dislocations intersect at regions of the $\Sigma=7$ boundary.

When the misorientation approaches that of the $\Sigma=7$ boundary, the roles of $\Sigma=7$ and $\Sigma=13$ units interchange. For example, the structure of the $\Sigma=201$ boundary, which (for the reason of space) is not shown here, is analogous to that of the $\Sigma=79$ boundary with the structural units of the $\Sigma=13$ boundary replacing the units of the $\Sigma=7$ boundary and *vice versa*. The grain boundary dislocations intersecting in the regions of the $\Sigma=13$ boundary are now the DSC dislocations of the type $(1/14)[\bar{3}21]$, related to the $\Sigma=7$ coincidence.

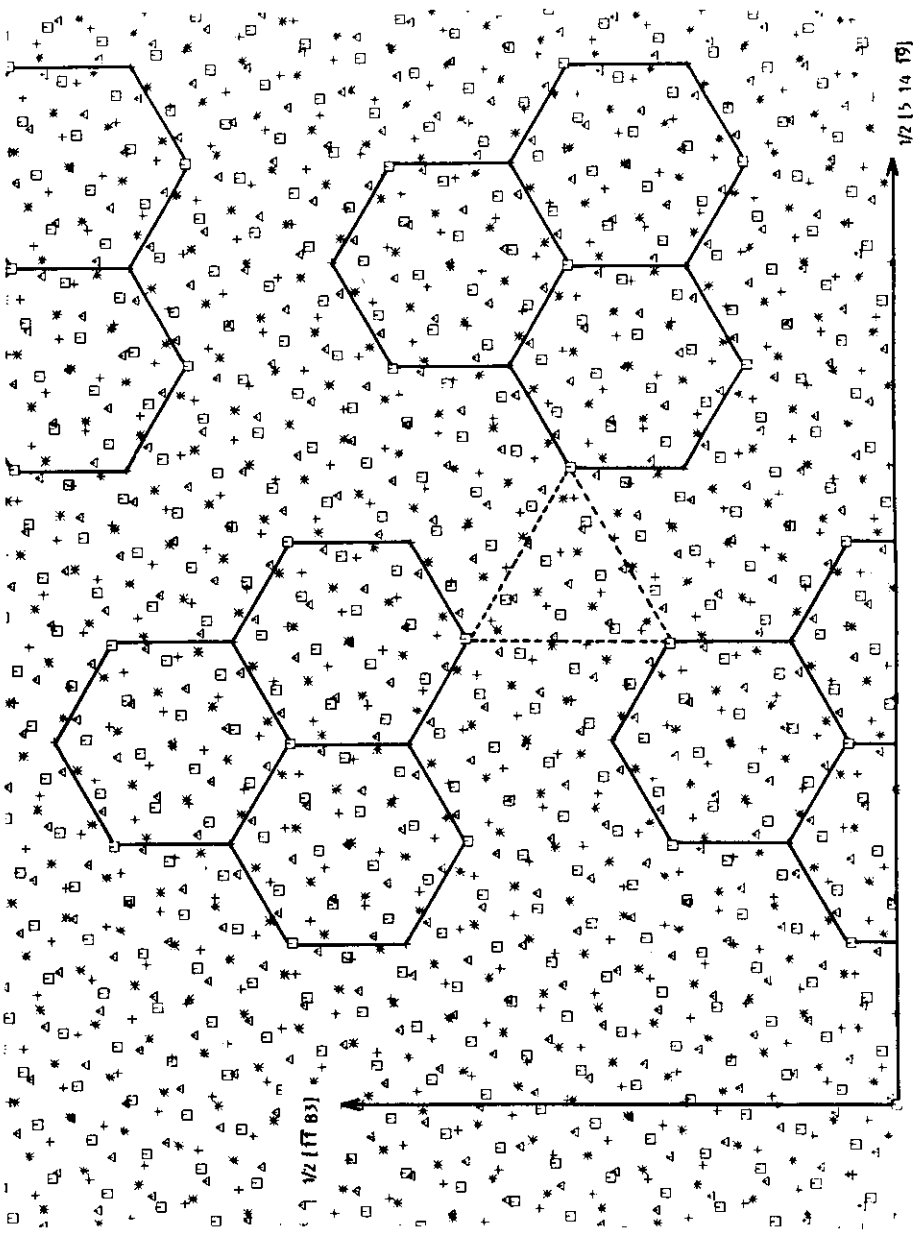

Fig. 9

Structure of the $\Sigma = 291$ boundary. Solid lines indicate slightly distorted $\Sigma = 13$ units surrounded by dislocations intersecting at $\Sigma = 39$ units (dashed line).

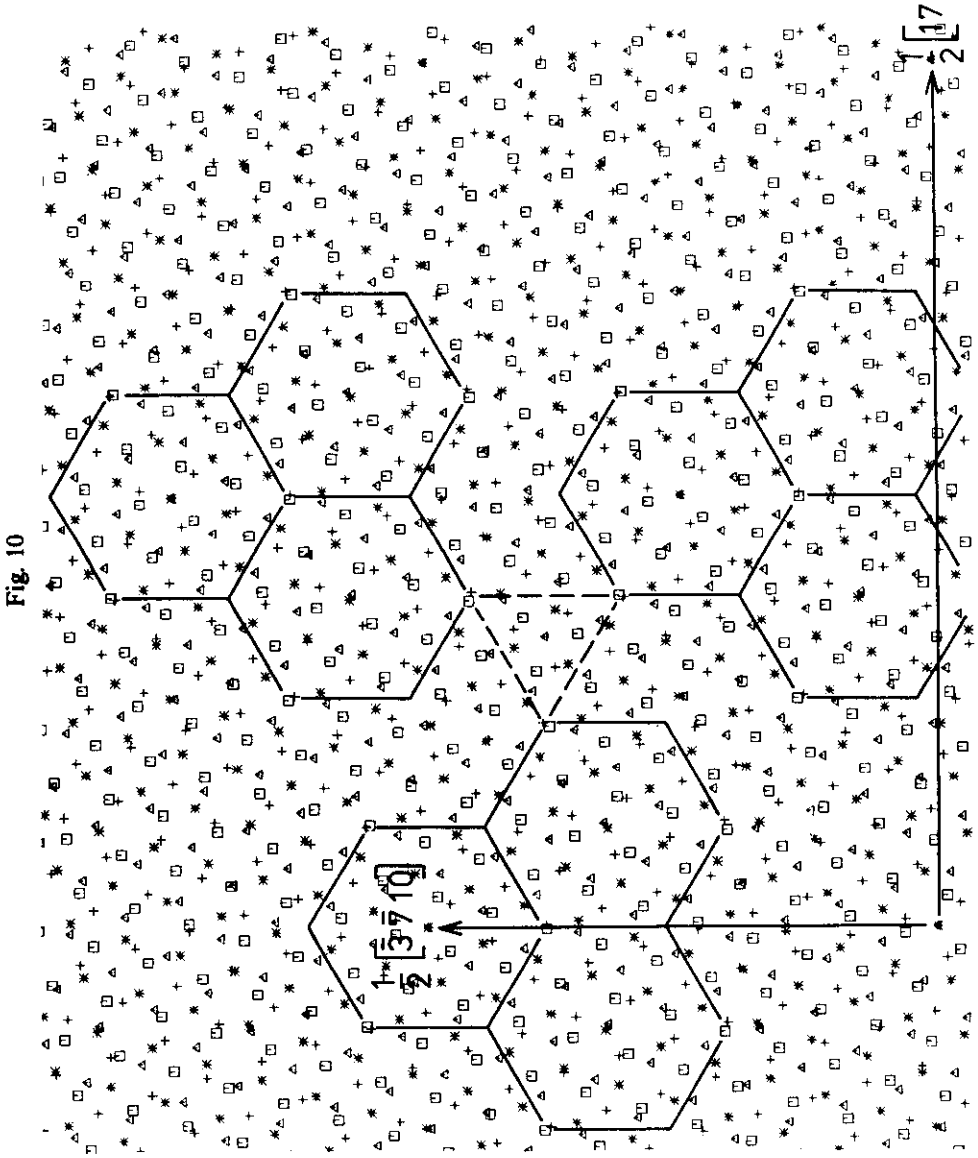

Fig. 10

Structure of the $\Sigma = 79$ boundary: solid lines indicate $\Sigma = 13$ units surrounded by dislocations intersecting at $\Sigma = 7$ units (dashed line).

4.5. *Misorientation range* $38{\cdot}21° < \Theta < 60°$

The structure of the $\Sigma = 49$ boundary has been found to consist of the units of the $\Sigma = 7$ structure surrounded by the network of DSC dislocations of the type $(1/14)[\bar{3}21]$ which intersect at the units of the $\Sigma = 3$ boundary. In the $\Sigma = 19$ boundary the ratio of the $\Sigma = 7$ and $\Sigma = 3$ units is 1 : 1 and the structure may be described either as $\Sigma = 7$ units surrounded by the network of $(1/14)[\bar{3}21]$ dislocations intersecting at $\Sigma = 3$ units or as $\Sigma = 3$ units surrounded by the network of DSC dislocations of the type $\frac{1}{6}[\bar{2}11]$ intersecting at $\Sigma = 7$ units. For the reason of space we do not show these structures here in detail. The $\Sigma = 61$ boundary, shown in fig. 11, represents a typical boundary with the misorientation close to that of $\Sigma = 3$. The triangular regions of the $\Sigma = 3$ twin are surrounded by the network of the DSC dislocations with the Burgers vectors of the type $\frac{1}{6}[\bar{2}11]$, which intersect at highly distorted units of the $\Sigma = 7$ boundary. As seen from fig. 11, the separation of the DSC dislocations in this network is equal to $|\frac{1}{4}[\bar{1}4\,13\,1]| = 4{\cdot}783a_0$, which agrees with Frank's formula (eqn. (7)). The alternate regions of the $\Sigma = 3$ twins are on different levels since $\frac{1}{6}\langle 112\rangle$ dislocations lying in the boundary are associated with steps of height $\frac{1}{3}[111]$.

§ 5. Discussion

In this paper we have studied the atomic structures of (111) twist boundaries and investigated the applicability of the structural unit model which has previously been established for tilt boundaries and (001) twist boundaries (Sutton and Vitek 1983, Schwartz *et al.* 1985). The calculations were carried out using two differing descriptions of interatomic forces, namely a pair potential for aluminium, for which the calculations were made at constant volume, and a many-body potential for gold, for which the calculations were performed at constant pressure. The atomic structures of all the boundaries studied were found to be very similar for both descriptions of atomic interactions. This suggests that the principal features of the structure of (111) twist boundaries found in this study are common to all f.c.c. metals. At the same time it supports the conclusion, discussed in a previous paper (Vitek and De Hosson 1986), that calculations employing pair potentials are fully capable of revealing the generic features of the structure of grain boundaries in metals. In general, large differences between calculations carried out using many-body potentials and pair potentials arise only if the coordination of atoms in the core of a defect is substantially different from that in the ideal crystal, and/or when large local expansions or contractions occur. Otherwise, the many-body potentials can be well approximated by effective pair potentials, as first pointed out by Finnis and Sinclair (1984). This suggests that in twist boundaries studied here neither large expansions nor large deviations in coordination occur, as has also been confirmed by detailed inspection of the calculated structures. This is also in full agreement with the recent study of Wolf and Lutsko (1989), who carried out calculations of the structure and energy of a number of different twist boundaries using many-body potentials of the embedded atom type (Daw and Baskes 1984) and the corresponding effective pair potentials, and found no substantial differences in these two cases. Nevertheless, the use of many-body potentials is advantageous in that the calculations can be carried out straightforwardly at constant pressure, and when evaluating the energy the uncertainties arising in the case of pair potentials due to the density-dependent term are alleviated.

The structural unit model, which establishes a relationship between structures of grain boundaries with different misorientations and relates the atomic structures and

Fig. 11

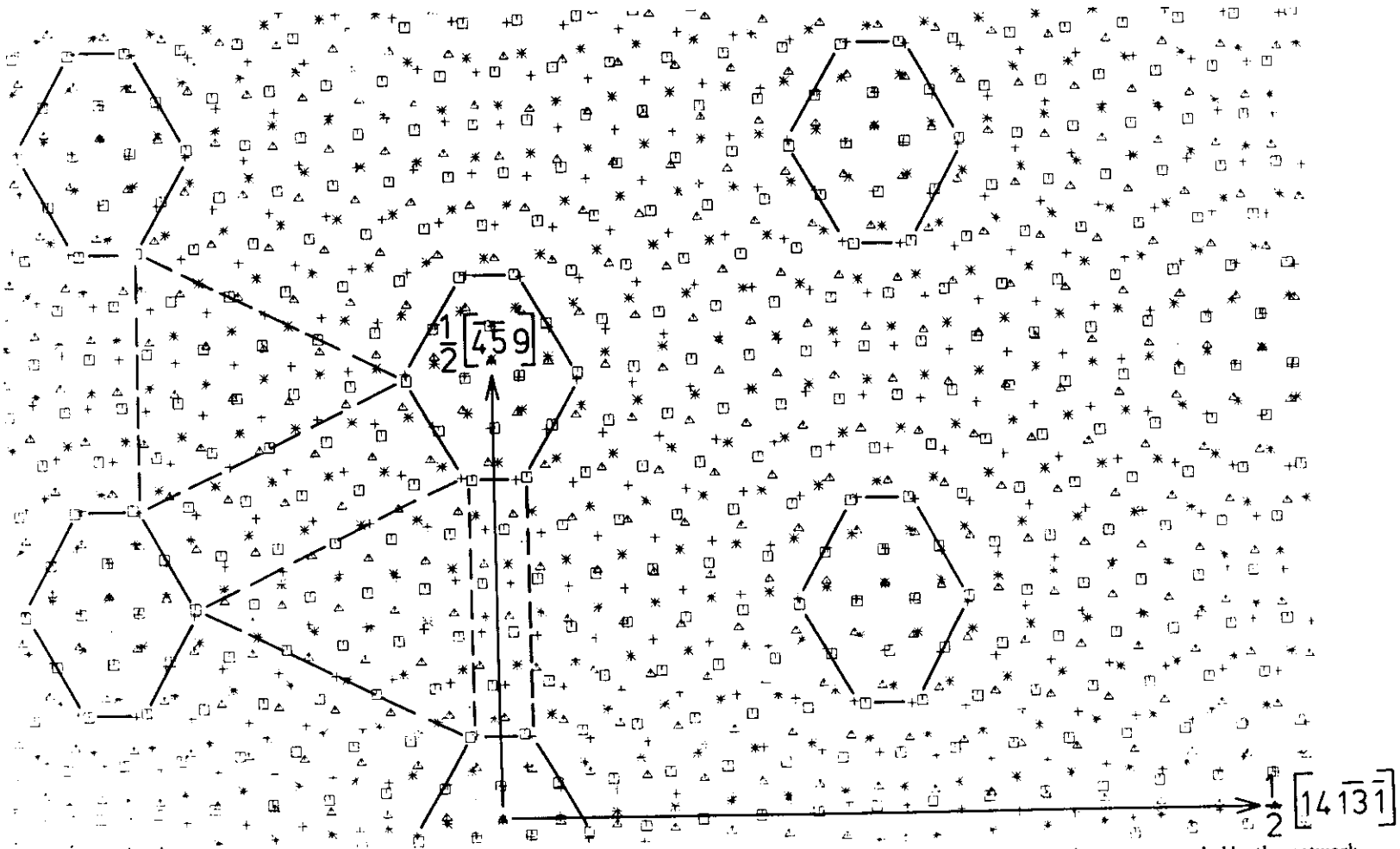

Structure of the $\Sigma = 61$ boundary: solid lines indicate distorted $\Sigma = 7$ units. Triangular regions (dashed line) of the $\Sigma = 3$ twin are surrounded by the network of the $\frac{1}{6}\langle 211\rangle$ DSC dislocations intersecting at $\Sigma = 7$ units.

corresponding dislocation contents of the boundaries, is an example of a generic result deduced on the basis of atomistic studies of grain boundary structures. Hence it is likely to be applicable to various types of tilt and twist boundaries. The results obtained here, indeed, show that structures of all the boundaries with misorientations between 0° and 21·79° ($\Sigma=21$) are composed of units of the ideal lattice and/or the $\frac{1}{6}\langle 112\rangle$ stacking fault on (111) planes, and units of the $\Sigma=21$ boundary. Similarly, structures of boundaries with misorientations between 21·79° and 27·8° ($\Sigma=13$), 27·8° and 38·21° ($\Sigma=7$) and 38·21° and 60° ($\Sigma=3$) can all be regarded as decomposed into units of the corresponding delimiting boundaries. The delimiting boundaries cannot be decomposed into any other structures and are thus favoured boundaries as defined by Sutton and Vitek (1983). In terms of the dislocation description the minority units can always be identified with intersections of dislocations forming a network possessing a three-fold symmetry and surrounding regions composed of majority units.

The dislocations present in the (111) twist boundaries are in most cases the DSC dislocations with the shortest possible Burgers vectors related to the CSL of the favoured boundary, the units of which are in the majority. There are, however, two notable exceptions. First, there are the low-angle boundaries in which the dislocations are the partial dislocations with Burgers vectors of the form $\frac{1}{6}\langle 112\rangle$. As first suggested by Amelinckx (1964), the low-angle (111) twist boundary could be regarded as a hexagonal network of $\frac{1}{2}\langle 110\rangle$ dislocations. However, in a $\{111\}$ plane these dislocations can, of course, dissociate into Shockley partials and it has been proposed by Scott and Goodhew (1981) that it is more favourable for every other node of the $\frac{1}{2}\langle 110\rangle$ dislocations to dissociate, thus forming a triangular network of $\frac{1}{6}\langle 112\rangle$ partials. This is indeed what has been found in our calculations and observed in gold using TEM (Scott and Goodhew 1981). This is also consistent with the earlier TEM observations of Schober and Balluffi (1969). Nevertheless, it should be mentioned that the interpretation of the contrast from dislocation networks in low-angle boundaries is complicated by the superposition of strain contrast from the network and interference (moiré) effects associated with the misorientation at the boundary. It has been shown (Hamelink and Schapink 1981, De Hosson *et al.* 1986) that, depending on the exact diffraction condition, the superposition may give rise to a hexagonal as well as a triangular type of contrast. This implies that the observation of a triangular network contrast cannot necessarily be interpreted in terms of the dissociation of a hexagonal network of screw dislocations as suggested by Scott and Goodhew (1981).

The second exception is the $\Sigma=43$ boundary in which the grain boundary dislocations with the Burgers vectors $(1/14)\langle 541\rangle$ and $(1/14)\langle 321\rangle$ are present, rather than the DSC dislocations with the shortest possible Burgers vector related to $\Sigma=21$, $(1/42)\langle 541\rangle$. The latter dislocations, while having a small Burgers vector, are associated with a large step of height $\frac{1}{3}\langle 111\rangle$ and it is, apparently, energetically more favourable when no steps are present in the boundary, even though the corresponding grain boundary dislocations must have in this case larger Burgers vectors. However, this feature of the grain boundary structure is not general, indeed, the $(1/42)\langle 541\rangle$ DSC dislocations have been found in the $\Sigma=67$ boundary. Whether dislocations possessing a short Burgers vector but associated with a step, or stepless dislocations with a longer Burgers vector, are energetically more favourable depends on the core structure of these dislocations. The present calculations suggest that for misorientations close to that of $\Sigma=21$, DSC dislocations without a step will be present for misorientations smaller than 21·79°, whilst dislocations associated with a step will be present for misorientations larger than 21·79°. Unfortunately, no electron microscope

observations of dislocations in (111) twist boundaries with misorientations close to that of $\Sigma = 21$ have been made.

Steps are similarly associated with $\frac{1}{6}\langle 112\rangle$ DSC disclocations present in the boundaries with the misorientation close to that of $\Sigma = 3$, as seen, for example, in the case of the $\Sigma = 61$ boundary (fig. 11). A number of experimental TEM observations of $\{111\}$ twist boundaries with misorientations close to that of the $\Sigma = 3$ twin have been reported (Erlings and Schapink 1977, 1978, Hamelink and Schapink 1981, Scott and Goodhew 1981, De Hosson *et al.* 1986) and the observed dislocation configurations generally agree with the present calculations. Experimentally a triangular network of secondary GBDs with dislocation spacings in the range of 10–80 nm was observed in artificially fabricated bicrystals of gold. In the recent study of the Burgers vectors of secondary GBDs in high-angle grain boundaries near $\Sigma = 9$, 27 and 81 in specimens prepared from a bulk polycrystalline Cu–6 at.% Si alloy (Forwood and Clarebrough 1985, 1986), several twin boundaries near $\Sigma = 3$ twin were observed to contain networks of secondary GBDs with spacings of 300 nm. In contrast to the aforementioned observations and to our calculations, the latter coarse networks are hexagonal and triangular cells were not observed. However, as pointed out by Forwood and Clarebrough (1986), the steps associated with the hexagonal network could involve a small departure from the (111) plane giving a tilt component to the boundary.

The calculated misorientation-dependence of the grain boundary energy is in full agreement with the dislocation picture deduced on the basis of the atomic structure. Following the Read–Schockley type model described in §2, cusps occur at misorientations corresponding to the reference structures, and, as seen from fig. 1, these can be identified with the favoured boundaries found from structural considerations. As discussed in a previous study of the (001) twist boundaries (Vitek 1988), the shape of the cusps depends strongly on the energy, E_c, and the core radius, r_0, of the grain boundary dislocations. These have been determined in detail for the (001) twist boundaries but not in the present case, since an accurate determination of these quantities would require detailed atomistic calculations of much longer period boundaries with large values of Σ, as was done for the (001) twist boundaries (Vitek 1988). The depth of the cusps depends principally on the energy of the reference structure, γ_0. A very deep cusp occurs, therefore, at the misorientation corresponding to $\Sigma = 3$, since the coherent twist boundary possesses much lower energy than the other favoured boundaries. Nevertheless, the cusps associated with other favoured boundaries are well defined. This is in contrast with the case of (001) twist boundaries where the cusp of the same type is observed only for $\Sigma = 5$, while for the other favoured boundaries ($\Sigma = 13$ and 17) the cusps are either very shallow or appear as inflections rather than as well defined minima on the energy against misorientation curve. Hence any experimental study depending on the presence of cusps, such as the rotating ball experiments of Sautter, Gleiter and Bäro (1977) or rotating particle experiments of Chan and Balluffi (1985), should reveal their presence for twist boundaries on (111) much more readily than for (001).

ACKNOWLEDGMENTS

This research was supported by The Foundation for Fundamental Research on Matter (F.O.M.-Utrecht) and has been made possible by financial support from The Netherlands Organization of Research (N.W.O.-The Hague) and in part by the National Science Foundation, MRL Program under Grant no. DMR85-19059 (VV).

References

Ackland, G. J., Tichy, G., Vitek, V., and Finnis, M. W., 1987, *Phil. Mag.* A, **56**, 735.

Amelinckx, S.: *The direct observation of dislocations, Solid State Physics*, Suppl., **6**, p. 3.

Balluffi, R. W., 1982, *Metall. Trans.* A, **13**, 2069.

Balluffi, R. W., Rühle, M., and Sutton, A. P., 1987, *Mater. Sci. Engng*, **89**, 1.

Bleris, G. L., Delavignette, P., 1981, *Acta crystallogr.* A, **37**, 779.

Chan, S. W., and Balluffi, R. W., 1985, *Acta metall.*, **33**, 1113.

Dagens, L., Rasolt, M., and Taylor, R., 1975, *Phys. Rev.* B, **11**, 2726.

Daw, M. S., and Baskes, M. I., 1984, *Phys. Rev.* B, **29**, 6443.

De Hosson, J. Th. M., Schapink, F. W., Heringa, J. R., and Hamelink, J. J. C., 1986, *Acta metall.*, **34**, 1051.

De Hosson, J. Th. M., and Vitek, V., 1987, *Chemistry and Physics of Fracture*, edited by R. M. Latanision and R. H. Jones (Dordrecht: Martinus Nijhoff), p. 363.

Doni, E. G., Bleris, G. L., Karakostas, Th., Antonopoulos, J. G., and Delavignette, P., 1985, *Acta crystallogr.* A, **41**, 440.

Duesberry, M. S., Jacucci, G., and Taylor, R., 1979, *J. Phys.* F, **9**, 413.

Erlings, J. G., and Schapink, F. W., 1977, *Scripta metall.*, **11**, 427; 1978, *Phys. Stat. sol.* (a), **46**, 653.

Finnis, M. W., Sinclair, J. E., 1984, *Phil. Mag.*, **50**, 45.

Forwood, C. T., and Clarebrough, L. M., 1985, *Aust. J. Phys.*, **38**, 449; 1986, *Phil. Mag.* A, **53**, L31.

Frank, F. C., 1950, *Symposium on the Plastic Deformation of Crystalline Solids*, (ONR Pittsburgh), p. 150.

Hamelink, J. J. C., and Schapink, F. W., 1981, *Phil. Mag.* A, **44**, 1229.

Hirth, J. P., and Lothe, J., 1982, *Theory of Dislocations*, (New York: Wiley).

Ishida, Y., (editor), 1986, *Grain Boundary Structure and Related Phenomena, Trans. Japan Inst. Metals*, **27**, No. 1.

King, A. H., 1982, *Acta metall.*, **30**, 419.

Pettifor, D. G., and Ward, M. A., 1984, *Solid St. Commun.*, **49**, 291.

Read, W. T., and Shockley, W., 1950, *Phys. Rev.*, **78**, 275.

Rühle, M., Balluffi, R. W., Fischmeister, H., and Sass, S. L., (editors), 1985, *International Conference on the Structure and Properties of Internal Interfaces, J. Phys., Paris*, **46**, C4.

Sass, S. L., and Raj, R., (editors), 1988, *Interface Science and Engineering '87, J. Phys., Paris*, (to be published).

Sautter, M., Gleiter, H., and Bäro, G., 1977, *Acta metall.*, **25**, 467.

Schwartz, D., Sutton, A. P., and Vitek, V., 1985, *Phil. Mag.* A., **51**, 499.

Schwartz, D., Bristowe, P. D., and Vitek, V., 1988, *Acta metall.*, **36**, 675.

Schober, T., and Balluffi, R. E., 1969, *Phil. Mag.*, **20**, 511.

Scott, R. F., and Goodhew, P. J., 1981, *Phil. Mag.* A, **44**, 373.

Sutton, A. P., 1982, *Phil. Mag.* A, **46**, 171; 1984, *Int. Metals Rev.*, **29**, 377; 1988, *Acta metall.*, **36**, 1291.

Sutton, A. P., and Vitek, V., 1983, *Phil. Trans. R. Soc. London*, A, **309**, 1.

Vitek, V., 1987, *Scripta metall.*, **21**, 711.

Vitek, V., and De Hosson, J. Th. M., 1986, *Computer-Based Microscopic Description of the Structure and Properties of Materials*, edited by J. Broughton, W. Krakow and S. T. Pantelides, *Mater. Res. Soc. Symp.*, **63**, 137.

Vitek, V., Sutton, A. P., Smith, D. A., and Pond, R. C., 1980, *Grain Boundary Structure and Kinetics*, edited by R. W. Balluffi, (Ohio: American Society for Metals), p. 115.

Wang, G.-J., Vitek, V., and Sutton, A. P., 1984, *Acta metall.*, **32**, 1093.

Wolf, D., and Lutsko, J. F., 1989, *Atomistic Modeling of Materials: Beyond Pair Potentials*, edited by D. J. Srolovitz and V. Vitek, (New York: Plenum).

Yoo, M. H., Briant, B. L., and Clark, W. A. T., (editors), 1988, *Interfacial Structure and Design, Mater. Res. Soc. Symp.*, (to be published).

PART-I-6

Reprinted from

ACTA METALLURGICA

Vol. 36, *No.* 10, *pp.* 2729–2741

ATOMIC STRUCTURE OF STOICHIOMETRIC AND NON-STOICHIOMETRIC GRAIN BOUNDARIES IN A_3B COMPOUNDS WITH $L1_2$ STRUCTURE

J. J. KRUISMAN, V. VITEK and J. TH. M. DE HOSSON

Department of Applied Physics, Materials Science Centre, University of Groningen, Nijenborgh 18, 9747 AG Groningen, The Netherlands

PERGAMON PRESS

OXFORD · NEW YORK · BEIJING · FRANKFURT

SÃO PAULO · SYDNEY · TOKYO · TORONTO

1988

Acta metall. Vol. 36, No. 10, pp. 2729–2741, 1988
Printed in Great Britain.

0001-6160/88 $3.00 + 0.00

ATOMIC STRUCTURE OF STOICHIOMETRIC AND NON-STOICHIOMETRIC GRAIN BOUNDARIES IN A_3B COMPOUNDS WITH $L1_2$ STRUCTURE

J. J. KRUISMAN, V. VITEK† and J. Th. M. De HOSSON
Department of Applied Physics, Materials Science Centre, University of Groningen, Nijenborgh 18, 9747 AG Groningen, The Netherlands

(*Received* 28 *September* 1987; *in revised form* 15 *February* 1988)

Abstract—Pair potentials are employed to investigate the similarities and differences between the boundaries in pure metals and $L1_2$ ordered compounds of the A_3B type. Symmetrical $\Sigma = 5$ (310) and (210) [001] tilt boundaries have been studied in detail. In addition, a limited study of the $\Sigma = 73$ (830) boundary has also been performed. It turns out that the concepts of structural units and multiplicity of boundary structures, originally developed for pure metals, are still applicable. In general, the atomic structures of the boundaries in A_3B–$L1_2$ compounds appear to be topologically similar to the structures of the boundaries of the same type in single-component f.c.c. materials. However, the multiplicity of boundary structures is much more extensive compared to pure materials since structures may differ not only topologically but also compositionally. The structural units in the stoichiometric boundaries are, in general, more distorted than those of either A or B rich boundaries (with respect to A_3B stoichiometry). Away from stoichiometry the structures resemble more closely the corresponding structures in single component systems. Possible consequences of these structural features for the grain boundary brittleness of the $L1_2$ compounds are discussed.

Résumé—Nous utilisons des potentiels de paire pour étudier les similitudes et les différences entre les joints dans les métaux purs et les points dans les composés ordonnés $L1_2$ du type A_3B. Nous avons étudié en détail les joints de flexion symétriques $\Sigma = 5$ (310) et (210) [001]. Nous avons également étudié, mais de façon moins approfondie, le joint $\Sigma = 73$ (830). Il ressort de ces études que les concepts d'unités structurales et de multiplicité de structures des joints, développés initialement pour les métaux purs, sont encore applicables. En général, les structures atomiques des joints dans les composés A_3B–$L1_2$ présentent la même topologie que les structures des joints du même type dans les matériaux cfc à un seul constituant. Cependant, la multiplicité des structures de joints est bien plus élevée que pour les matériaux purs, car les structures peuvent différer non seulement en topologie, mais encore en composition. Les unités structurales dans les joints stoechiométriques sont en général plus déformées que les unités dans les joints riches en éléments A ou B (par rapport à la stoechiométrie A_3B). En dehors de la stoechiométrie, les structures ressemblent davantage aux structures correspondantes des systèmes à un seul constituant. Nous discutons les conséquences possibles de ces caractéristiques structurales sur la fragilité intergranulaire des composés $L1_2$.

Zusammenfassung—Die Ähnlichkeiten und Unterschiede zwischen Korngrenzen in reinen Metallen und in $L1_2$-geordneten Legierungen vom Typ A_3B werden mit Paarpotentialen untersucht. Ausführlich wurden symmetrische Korngrenzen $\Sigma = 5$ (310) und Kippkorngrenzen (210) [001] analysiert. Die Korngrenze $\Sigma = 73$ (830) wurde außerdem kurz untersucht. Es ergibt sich, daß die Konzepte der strukturellen Einheiten und der Multiplizität der Korngrenzstrukturen, die ursprünglich für reine Metalle entwickelt worden waren, noch anwendbar sind. Im allgemeinen scheinen die atomaren Strukturen der Korngrenzen in A_3B–$L1_2$-Legierungen topologisch den Strukturen der Korngrenzen desselben Typs in einkomponentigen kfz. Metallen zu ähneln. Dagegen ist die Multiplizität der Korngrenzstrukturen gegenüber denen in reinen Metallen viel ausgeprägter, da die Strukturen sich nicht nur topologisch sondern auch in der Zusammensetzung unterscheiden können. Die strukturellen Einheiten in stöchiometrischen Korngrenzen sind im allgemeinen stärker verzerrt als diejenigen in den A- oder B-reichen Korngrenzen (bezogen auf A_3B-Stöchiometrie). Außerhalb der Stöchiometrie entsprechen die Strukturen den entsprechenden Strukturen der einkomponentigen Systeme besser. Mögliche Konsequenzen dieser strukturellen Eigenschaften für die Korngrenzsprödigkeit der $L1_2$-Legierungen werden diskutiert.

1. INTRODUCTION

In recent years the atomic structure of grain boundaries in metals and ionic crystals has been studied extensively using computer simulations in which blocks of many atoms are relaxed to attain the minimum energy configuration under the condition that a chosen boundary is present in the middle of the block (for reviews see e.g. [1–5]). In these calculations pair-potentials are usually employed to describe the interatomic forces. While this approximation is not

†On leave from Department of Materials Science and Engineering, University of Pennsylvania, Philadelphia, PA 19104–6272, U.S.A.

generally sufficient for evaluation of total energies of solids, calculations employing pair-potentials are capable of revealing important structural features which are insensitive to the details of interatomic forces [6]. Such features are either related to the crystallography of grain boundaries and adjoining grains, though not determined purely crystallographically, or show possible trends and variability of the boundary structures in different materials. An example of the former is the structural unit model for the low coincidence boundaries [2–4, 7–9] and of the latter the recently discussed multiplicity of boundary structures [10–12]. Furthermore, features common to grain boundaries in different materials crystallizing in the same crystal structure can be found on the basis of these studies. Many structural features revealed by such calculations have been confirmed experimentally (e.g. [1, 2, 12–15]) and their results represent, together with crystallographic approaches such as coincidence site lattice (csl) and O-lattice theory, the principal source of our present understanding of the basic features of the atomic structure of grain boundaries [1, 15].

Most of the atomistic calculations of grain boundary structures were made for single component systems. However, many important boundary phenomena are strongly affected by alloying. For example, it has been known for a long time that in disordered alloys segregation of alloying elements and impurities to grain boundaries often strongly increases their propensity to fracture (e.g. [16]). Recently, it has been found that in f.c.c. based $L1_2$ compounds, such as Ni_3Al, which are ductile in single crystalline form, are very susceptible to intergranular fracture (e.g. [17, 18] and other papers in [19, 20]). This is rather unfortunate since they are attractive materials for high temperature applications. It has been suggested by several authors [18, 21, 22] that brittleness at grain boundaries is an intrinsic property of these compounds, in contrast with pure metals and disordered alloys where intergranular fracture is always induced by segregation of impurities and/or alloying elements. At the same time it was found that variation of the stoichiometry of intermetallic compounds [21, 23, 24] as well as doping, for example, by boron in the case of Ni_3Al, may affect dramatically their ductility [17–26]. These strong compositional effects can be related either to electronic [21–24] or structural changes in the grain boundary region and investigation of the latter is one of the goals of this paper.

From the structural point of view, grain boundaries in $L1_2$ compounds have been studied in the last few years crystallographically, employing the CSL, O-lattice and group theoretical analyses [27–32]. A number of geometrical and symmetry related features which distinguish boundaries in compounds from those in mono-atomic materials, have been pointed out. One of these features is the structural multiplicity arising from possible different distributions of the two elements forming the compound, on different sublattices in the adjoining grains. This multiplicity, and its further enhancement by changes in stoichiometry, are also investigated in the present paper. Studies of the atomic structure of grain boundaries in $L1_2$ compounds which take into account the atomic interactions and thus the energetics of the system, have so far been very limited. A model in which the atoms of the two different species forming the compound are treated as hard spheres of different radii, has recently been developed by Farkas and Rangarajan [33] and atomistic computer simulations have been performed by Chen *et al.* [34, 35] and Foiles [36].

A necessary precursor of any atomistic study is a physically reasonable description of interatomic forces. When a detailed description of properties of a specific material, e.g. a Ni–Al alloy, is required this can only be achieved in the framework of a full quantum mechanical treatment, for example, by employing the local density functional theory (e.g. [37, 38]). However, this treatment is still beyond the realm of present computers when considering extended defects which require that a large number of atoms is included in the relaxed block. On the other hand, a more modest aim, such as investigation of those boundary properties which are common to all the compounds crystallizing in the $L1_2$ structure may succeed even when employing a much more simplified description of interatomic forces. This approach was adopted in many atomistic studies of lattice defects (see e.g. [6] and papers in [39, 40]). For the case of $L1_2$ alloys such calculations were carried out using interatomic forces described by pair-potentials constructed such that the $L1_2$ structure is stable both mechanically and when compared with the corresponding disordered f.c.c. alloy, to study stacking faults, antiphase boundaries and dislocation cores [41–43]. Results of these calculations were then employed to explain very comprehensively the complex high and low temperature yielding behaviour of these materials [44–46]. The same philosophy has been adopted in the present paper. The pair potentials, constructed in [41] and used in the dislocation studies, are employed here to investigate the similarities or differences between the boundaries in pure metals and $L1_2$ ordered compounds of the A_3B type. For this purpose, symmetrical $\Sigma = 5$ (310) and (210) [001] tilt boundaries have been studied in detail and a limited study of the $\Sigma = 73$ (830) boundaries has been performed. The structures of these boundaries in a mono-atomic f.c.c. lattice were studied in the past by several authors (e.g. [1, 2, 10]) and a comparison of the corresponding structures is made in the present paper. The structural differences arising from the ordering tendency are then the principal topic of interest. At the same time we follow in more detail the structural multiplicity associated with different distributions and local concentrations of the two alloy components in the boundary region. Finally, we

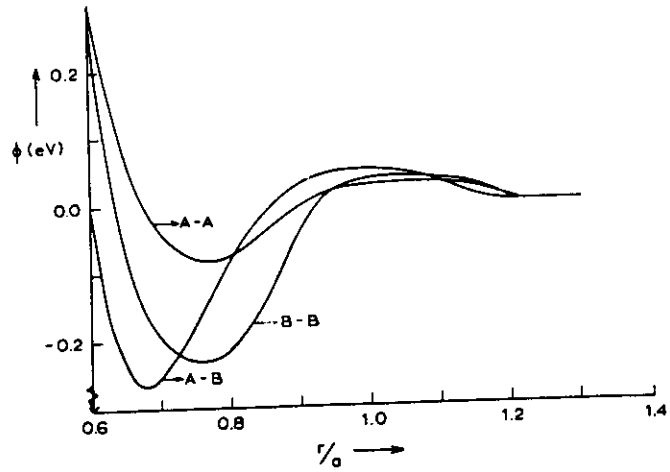

Fig. 1. Interatomic potentials of A–A, B–B, and A–B interactions.

discuss possible consequences of the structural features specific to the $L1_2$ compounds for the grain boundary brittleness.

2. INTERATOMIC POTENTIALS AND METHOD OF CALCULATIONS

The pair potentials used here, shown in Fig. 1, were not constructed to reproduce physical properties of a particular alloy but to describe a stable $L1_2$ structure with a relatively high ordering energy. They correspond to the potential set C-1 of Ref. [41] and the details of their construction are described in this paper. All three potentials are truncated with zero slope and curvature at $r/a = 1.219$, where a is the lattice parameter of the alloy. This is very close to the third nearest neighbour separation in the $L1_2$ structure. In the ideal $L1_2$ lattice the energy per atom A is $E_A = -0.629\,\text{eV}$ and the energy per atom B is $E_B = -1.4\,\text{eV}$. The Cauchy relations for the elastic constants are satisfied when these potentials are used and thus the density dependent term which generally occurs in the expression for the total energy of the system, can be set equal to zero. As shown in [41], these potentials ensure the mechanical stability of the $L1_2$ lattice with respect to both large expansions of the lattice and large shears on low index crystallographic planes. Furthermore, recent calculations of energies of antiphase boundaries on a variety of crystallographic planes, in which these potentials were used, show that these energies are always positive, though less anisotropic than what is commonly assumed [47].

The minimum of the potential describing the A–B interaction is at $r/a = 0.679$ a distance about 4% shorter than the separation of the first nearest neighbours. This potential is deeper than any of the two potentials describing A–A and B–B interactions and, clearly, formation of A–B pairs at nearest neighbour separations is energetically favourable. Hence, in this model ordering is favoured due to the nearest neighbour interactions, which is a common assumption in theoretical studies of ordering. The ordering energy, evaluated according to Ref. [48], is $-0.924\,\text{eV}$ and the corresponding critical temperature of ordering is then 1719 K. This is a relatively high ordering energy but not unreasonable for materials which do not undergo an order–disorder transformation before melting, such as Ni_3Al, the melting temperature of which is 1670 K.

The minimum of the B–B potential is at $r/a = 0.758$ and the difference between the positions of the minima of B–B and A–B potentials can be taken as a measure of the difference between radii of atoms A and B. In the present case this difference is about 12% and thus the potentials describe an $L1_2$ structure composed of species the atomic radii of which differ by this amount. As discussed, for example in [33], such a difference in atomic sizes is a reasonable assumption in Ni_3Al but it is expected to be much smaller, for instance, in Cu_3Au.

Using these potentials we have also calculated the energy changes associated with creation of antisite defects in the $L1_2$ structure. These correspond to the replacement of one of the A atoms by a B atom and vice versa. When evaluating the energies of antisite defects we have taken into account the relaxation that occurs in their vicinity. This calculation was carried out using the same relaxation procedure as in the studies of grain boundaries. Hence, a widely separated periodic array of antisite defects was always considered. The energies of the antisite defects calculated in this way are, when A is replaced by B, $E_{B\text{-}A} = -1.55\,\text{eV}$, and when B is replaced by A, $E_{A\text{-}B} = +2.213\,\text{eV}$. Although $E_{B\text{-}A}$ is negative ordering is still favoured since pairs of anti-site defects occur in the disordered state and the energy of a pair of such defects is positive. The positive value of $E_{A\text{-}B}$ implies that in the bulk, it is energetically unfavourable to deviate away from the stoichiometry towards the surplus of A while the negative value of $E_{B\text{-}A}$ implies that the deviation away from the stoichiometry which leads to the surplus of B, is energetically favoured.

This is the same trend implied, for example, for Ni_3Al from the measured concentration dependence of the enthalpy of mixing in Ni–Al alloys [45].

The method of calculation was basically the same as in a number of previous studies and has been described in detail elsewhere [8, 50]. A block consisting of the atomic coordinates of an unrelaxed $L1_2$ bicrystal, containing the chosen coincidence boundary, is first constructed in the computer using the basic geometrical rules of the CSL. The periodicity of the CSL parallel to the boundary plane is then maintained during the relaxation. A relaxed structure is found by minimizing the total internal energy with respect to all atomic positions subject to the constraint that the total volume of the block is constant. The relaxation procedure utilizes a standard gradient method. During the relaxation relative displacements of atomic layers parallel to the boundary, as well as individual atomic relaxations, are permitted and net relative translation of the two grains parallel to the boundary may occur. Different starting configurations corresponding to different distributions and concentrations of A and B atoms in the boundary region were used in order to investigate the variation of the boundary structure with local deviations from ideal stoichiometry.

In this paper we concentrate purely on the structural features and do not give values of their energies. The reason for this is two-fold. First, as explained above, the potentials used here do not represent any particular material and thus the absolute values of energies are not meaningful. Secondly, in ordered alloys, unlike in mono-atomic systems, the choice of the reference system with respect to which the energy is measured, is not unique if deviations away from the ideal stoichiometry are allowed.

3. CRYSTALLOGRAPHY OF GRAIN BOUNDARIES

The crystallographic, geometrical characteristics of grain boundaries in the $L1_2$ structure were studied by several authors [27–32] and we summarize here only those features which are important for the grain boundaries treated in this paper. The basic difference between grain boundaries in $L1_2$ and f.c.c. materials is that in the former case, boundaries with identical atom locations are different if the same atomic positions are occupied by different species. In any A_3B alloy with the $L1_2$ structure, there are two types of crystallographic planes: (i) planes which all contain three quarters of A atoms and one quarter of B atoms; (ii) planes, half of which contain only A atoms (α planes) and the other half an equal number of A and B atoms (β planes). The planes that meet at a boundary with a regular repeating structure must always be either type (i) or type (ii) [32, 51]. All the crystallographic planes that are parallel to the [001] direction are of type (ii) and, therefore, in the case of [001] tilt boundaries the planes parallel to the boundary are always of this type [32].

When neglecting the identity of atomic species, the $L1_2$ structure becomes the f.c.c. lattice. The f.c.c. lattice can be regarded as composed of four simple cubic sublattices and the $L1_2$ structure is then obtained if A atoms are placed on three of these sublattices and B atoms on the remaining one. When considering the crystallography of grain boundaries in $L1_2$ alloys, the approach adopted, for example in [27, 32], was to start from the boundary in the underlying f.c.c. structure and distribute then atoms A and B in all possible distinct ways onto the corresponding simple cubic sublattices in the upper and lower grains, respectively. In general, there is a maximum of 16 combinations but some of them may result in identical boundary structures. It was shown in [32] that there are eight distinct configurations in the case of [001] tilt boundaries. Four of these configurations are such that the stacking sequence of planes parallel to the boundary is everywhere $\ldots\alpha\beta\alpha\beta\alpha\beta\ldots$ so that stoichiometry is preserved in the block. However, in two of these configurations the stacking sequence $\ldots\alpha\beta\alpha\alpha\beta\alpha\beta\ldots$ occurs in the boundary region and in the other two the sequence $\ldots\alpha\beta\alpha\beta\beta\alpha\beta\ldots$ is found. In the former two structures, obtained f.i. by inserting an α plane into the stoichiometric sequence, there is a surplus of two A atoms in the boundary region, relative to the ideal stoichiometric situation. In the latter two structures obtained by removing an α plane from the stoichiometric sequence, there is a lack of two A atoms per period. Examples of these structures are shown in the following section.

In the crystallographic treatments of the boundary structures, it has been implicitly assumed that when considering either the lower or the upper grain separately, each of them is an ideal $L1_2$ single crystal. This condition determines uniquely the possible boundary configurations summarized above. However, the grain boundary region is topologically different from the ideal lattice and thus there is no *a priori* reason why in the vicinity of the boundary the A and B atoms could not be positioned such that deviations away from the ideal $L1_2$ structure occur in several planes adjacent to the boundary. Similarly, larger deviations from ideal stoichiometry than those mentioned above may occur locally. Which of these structures are stable and represent energetically favourable configurations can only be determined by atomistic simulations. This has been explored in the present study by varying distributions of A and B atoms as well as altering the local stoichiometry in initial boundary structures used as starting configurations in the relaxation calculations. Possible variability of the atomic configurations which involve various distributions of A and B species is very extensive and only a small number of all the possible configurations were considered here. However, general structural features associated with changes in local stoichiometry, appear to be well revealed by the cases studied here.

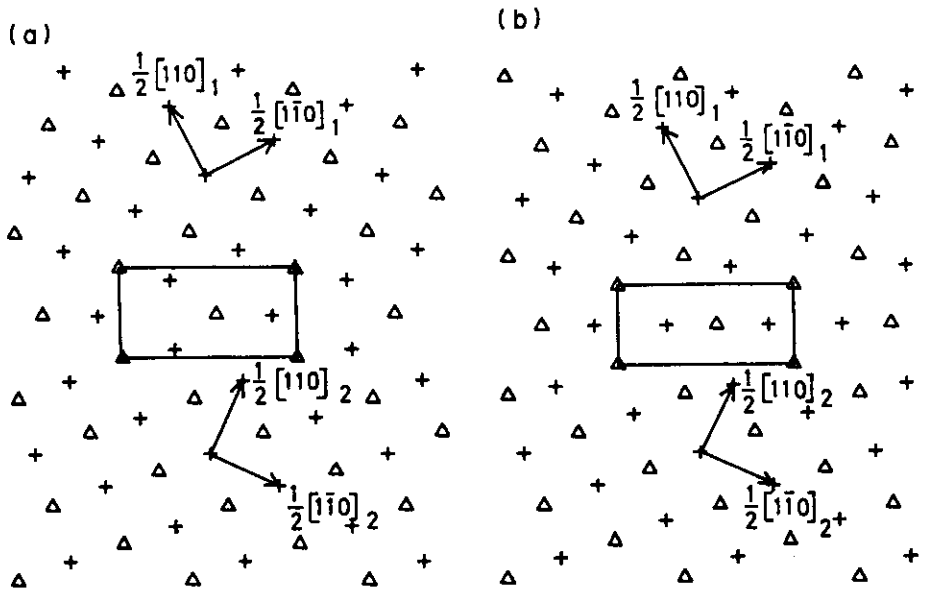

Fig. 2. (a,b) Structural units in the $\Sigma = 5$ (310) tilt boundary in f.c.c. material.

4. ATOMIC STRUCTURES OF GRAIN BOUNDARIES

4.1. Σ-5 tilt boundaries

The atomic structures of the $\Sigma = 5$ (310) and (210) tilt boundaries in a mono-atomic f.c.c. material were calculated in a number of studies (e.g. [8, 10, 52]). Two alternative structures which differ in the relative translations of the grains and possess somewhat different energies, were found in both cases; they are shown in Figs 2(a, b) and 3(a, b), respectively. In these and all the following figures, the triangles and crosses distinguish between the two (002) planes in each crystal period along the [001] tilt axis. The lines

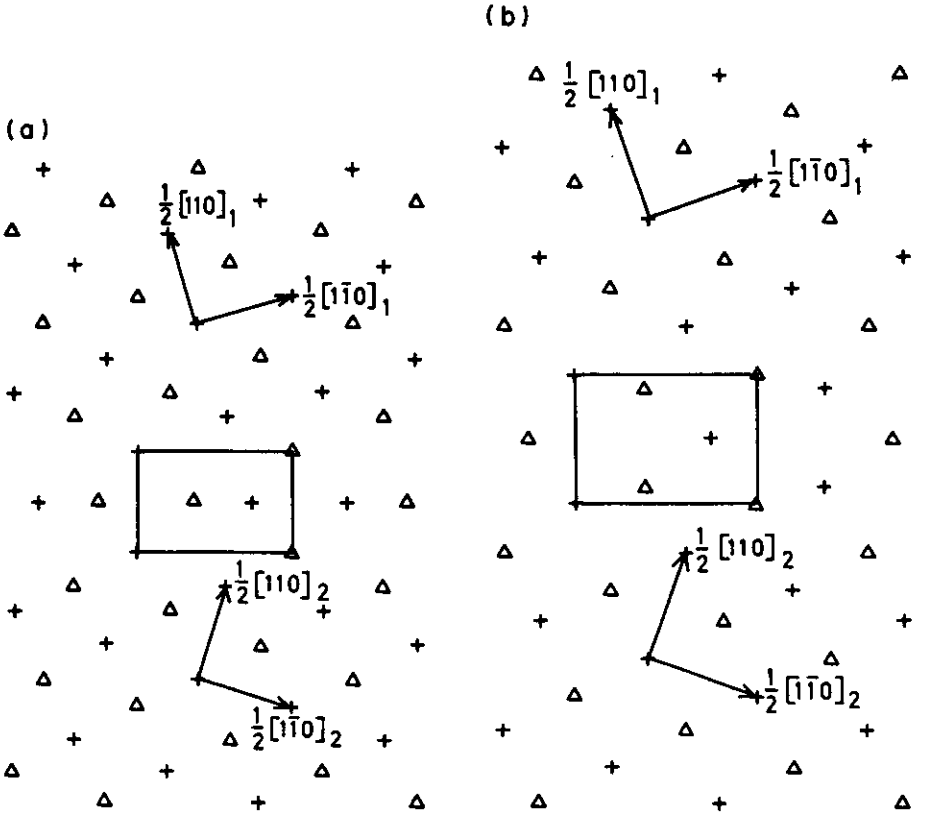

Fig. 3. (a,b) Structural units in the $\Sigma = 5$ (210) tilt boundary in f.c.c. material.

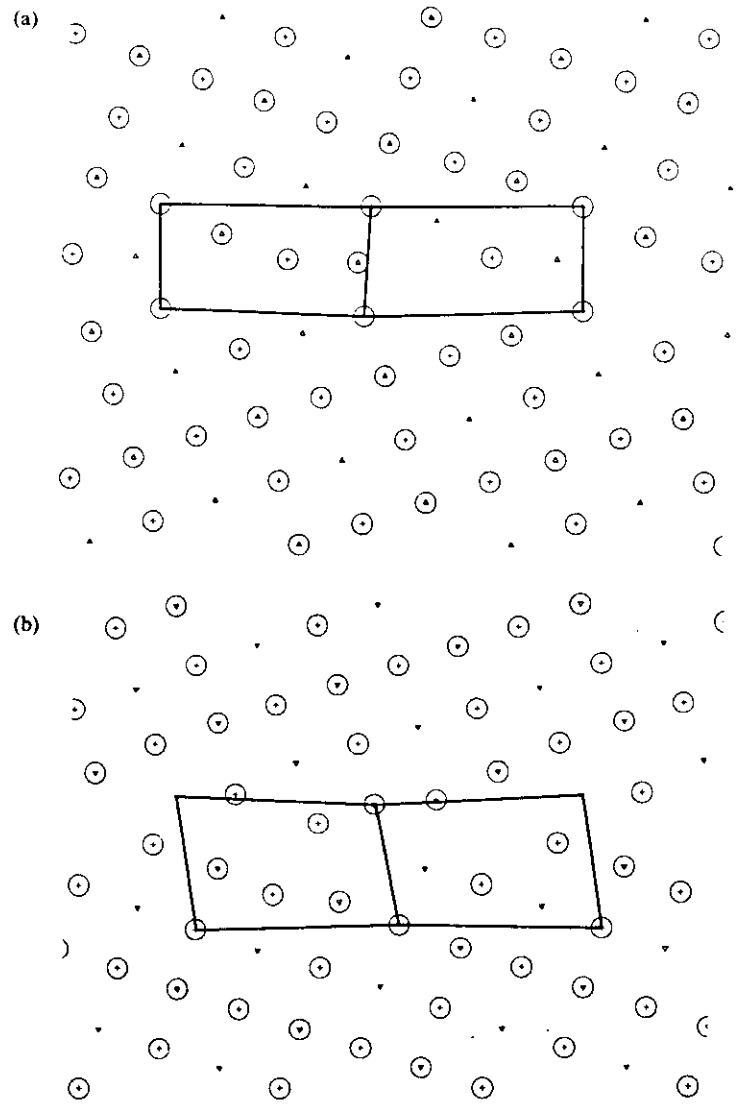

Fig. 4. (a,b) $\Sigma = 5$ (310) boundary structure in A_3B–Ll_2 with the stoichiometric composition.

drawn in Figs 2 and 3 indicate suitable units of these boundaries which contain sufficient numbers of atoms to typify the boundary structure. Corresponding units in other boundaries shown in this paper are denoted similarly. These units can then be found in high Σ long period boundaries the structures of which are composed of units of low Σ short period boundaries following the structural unit model [2, 8, 10].

A number of stoichiometric (310) boundary structures have been studied. The starting configurations were geometrically constructed boundaries in which the sequence of layers parallel to the boundary is $\ldots\alpha\beta\alpha\beta\alpha\beta\ldots$, as well as structures in which this sequence is $\ldots\alpha\beta\alpha\alpha\beta\beta\alpha\beta\ldots$. Several of these structures were found to be metastable. However, in the relaxed structures, atomic layers parallel to the boundary are, in general, no more distinct in the boundary core but interpenetrate, and, therefore, similar structures often resulted when starting with different initial configurations. Two typical structures of the stoichiometric boundaries are shown in Fig. 4(a, b). The circled symbols in these and all the following figures represent A atoms; B atoms are denoted by single symbols. The structural units of these boundaries are again denoted by solid lines. In the following we shall consider two structural units as topologically equivalent if they contain the same number of atoms, regardless of the type of species, each of which possesses the same number of nearest neighbours. The separations of the neighbouring atoms in topologically equivalent units are, however, generally different. Hence the units of the boundary shown in Fig. 4(a) can be regarded topologically as distorted units of the structure shown in Fig. 2(b), and the units of the boundary shown in Fig. 4(b) as distorted units of the structure shown in Fig. 2(a).

Typical (310) structures with surplus of two and

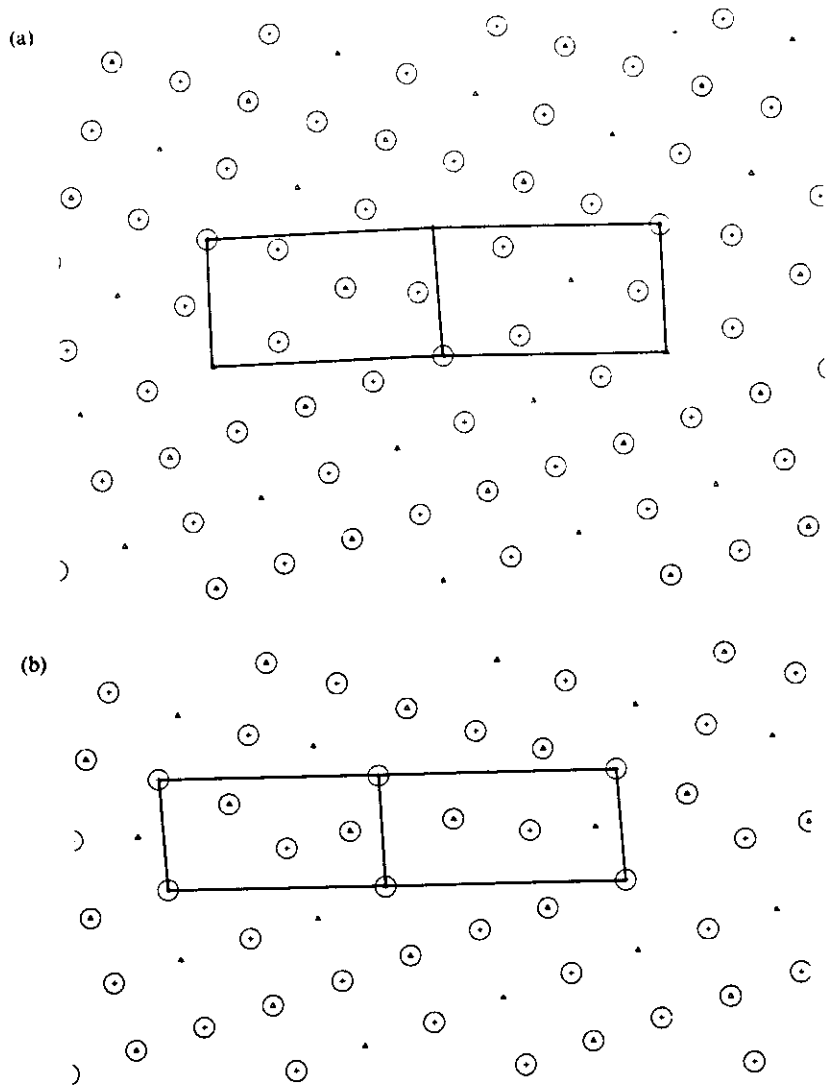

Fig. 5. $\Sigma = 5$ (310) boundary structure in A_3B–$L1_2$ with a surplus of two A atoms per period (a) and of four A atoms per period (b) relative to the stoichiometric concentration.

four A atoms per boundary period are shown in Fig. 5(a) and (b), respectively. Structural units of these boundaries are topologically, similar to the units depicted in Fig. 2(a) and 2(b), respectively. Typical structures with a lack of 2 and 4 A atoms per boundary period are shown in Fig. 6(a) and 6(b), respectively. The structural units of these boundaries are again topologically similar to the units shown in Fig. 2(a, b). When increasing the concentration of either A or B in the boundary even further the structures have been found to be topologically more and more similar to those shown in Fig. 2.

The atomic structures of (310) tilt boundaries of $L1_2$ alloys appear to be in most cases topologically similar to the corresponding structures in f.c.c. materials. However, large distortions away from these structures occur for stoichiometric boundaries and the distorted structures usually contain large "holes" (e.g. Fig. 4). As seen from Figs 5 and 6, the distortions then decrease and boundaries in $L1_2$, in general, resemble more closely those in f.c.c., as the surplus of either A or B in the boundary region increases. However, the decrease of distortions is not a monotonous function of the surplus of A or B [see e.g. Figs 5(b) and 6(b)], in particular at not too high values of the surplus.

The structural characteristics of (210) boundaries have been found to be very similar to those of (310) boundaries but the distortions away from the corresponding f.c.c. structures are, in general, smaller. Two typical (210) boundary structures with the stoichiometric composition are shown in Fig. 7(a, b). The starting configuration of the structure shown in Fig. 7(a) was constructed geometrically as described in the previous section. In this case the sequence of the planes parallel to the boundary is $\ldots\alpha\beta\alpha\beta\alpha\beta\ldots$ and the relaxed structure is similar to the unrelaxed one. The starting configuration of this structure can

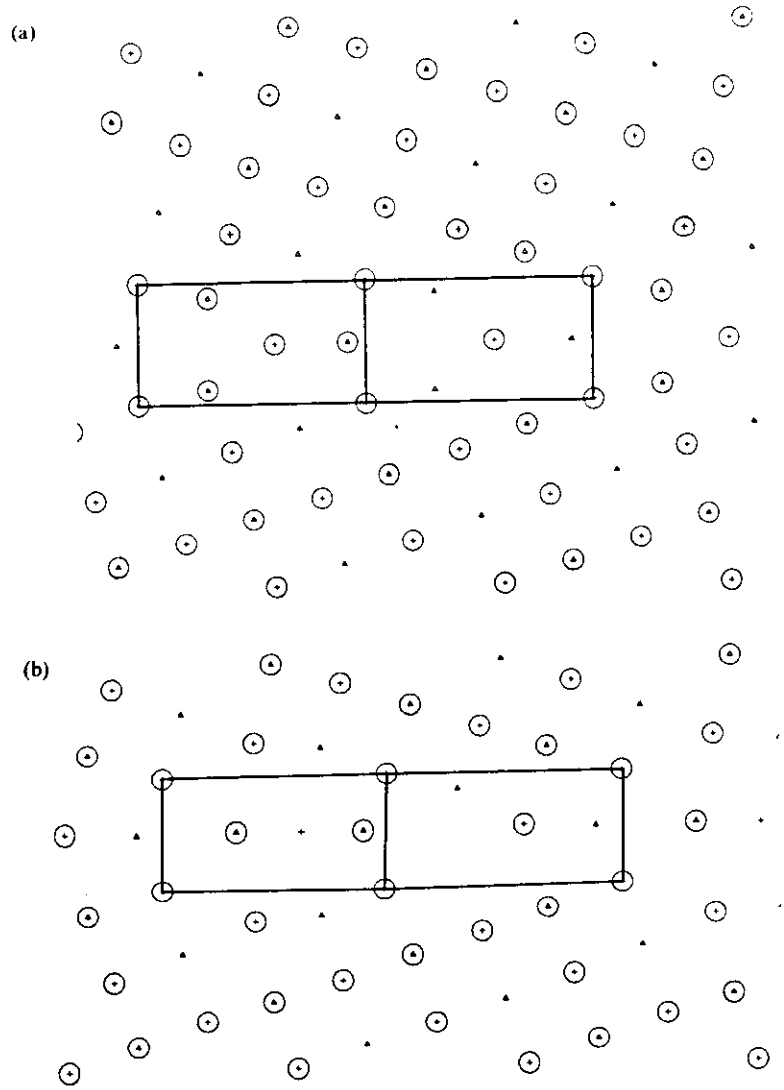

Fig. 6. $\Sigma = 5$ (310) boundary structure in A_3B–$L1_2$ with a lack of two A atoms per period (a) and a lack of four A atoms per period (b) relative to the stoichiometric concentration.

be found in Ref. [7] [Fig. 4(a)] and the same relaxed configuration of this boundary was also found by Chen *et al.* [34]. It is seen that the basic structural units are topologically similar to the units shown in Fig. 3(b). In the structure shown in Fig. 7(b) the order of the planes parallel to the boundary is $\ldots\alpha\beta(\alpha\beta)\alpha\alpha\beta\beta\alpha\beta\ldots$and it does not correspond to any of the geometrically constructed structures. (Interpenetrating planes in the relaxed configurations are set in parentheses). Structural units of this boundary are topologically similar to those of Fig. 3(a).

A structure with a surplus of two A atoms per period relative to the stoichiometric concentration, is shown in Fig. 8(a) and a structure with the surplus of four A atoms per period relative to the stoichiometric concentration is shown in Fig. 8(b). In all these structures and in another one (not shown here) with the surplus of eight A atoms per period, the structural units are topologically similar to those shown in Fig. 3(a, b). A structure with the lack of 2 A atoms per period relative to the stoichiometric concentration, is shown in Fig. 9. Its structural units are topologically similar to those shown in Fig. 3(a). A structure with the lack of 4 A atoms per period has also been calculated and it was found to be topologically very similar to that of Fig. 8. Topologically, the structural units of these boundaries are similar to the units shown in Fig. 3(a) but structures with units similar to those shown in Fig. 3(b) have also been found.

4.2. $\Sigma = 73$ (830) boundary

A large number of high Σ [001] symmetrical tilt boundaries in an f.c.c. material have been studied in [10]. Their structures all conform to the structural unit model but an extensive multiplicity of the structures of these boundaries arises due to multiplicity of the corresponding delimiting boundaries. For ex-

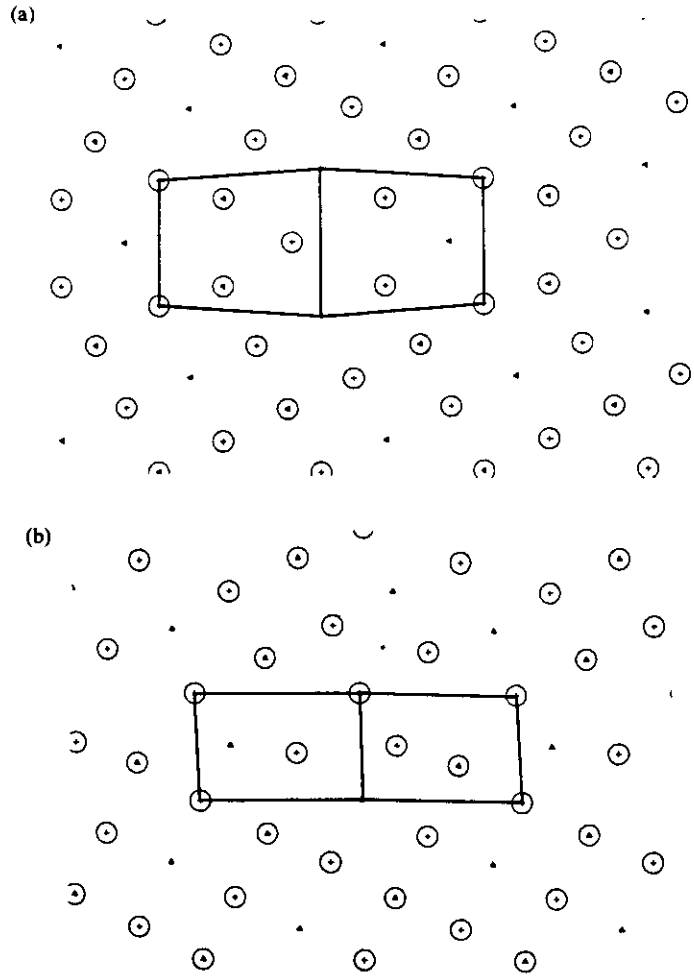

Fig. 7. (a,b) $\Sigma = 5$ (210) boundary structures in A_3B–$L1_2$ with the stoichiometric composition.

ample, following the structural unit model, every half period of the $\Sigma = 73$ (830) boundary consists of two units of the $\Sigma = 5$ (310) boundary and one unit of the $\Sigma = 5$ (210) boundary. Since there are two different structures of each of these delimiting boundaries (see also Figs 2 and 3) there are eight possible structures of the CSL periodic (830) boundary. All these structures were found to be metastable [10]. If the condition of the CSL periodicity is relaxed many long period structures and even non-periodic structures may be envisaged [11, 12]. However, the structures of these boundaries are still composed of well defined units of the delimiting boundaries and are not, therefore, random. In the case of an $L1_2$ alloy, the variety of possible structures of the delimiting boundaries is much larger since different structures do not differ only topologically but also compositionally. Hence, an even more extensive multiplicity of long period boundaries can be expected.

In the present paper only one long period boundary, $\Sigma = 73$ (830) has been studied, and even then only a small number of its possible structures. Three typical structures of the $\Sigma = 73$ boundary which differ both topologically and compositionally, are shown in Fig. 10(a–c). The structure in Fig. 10(a) corresponds to the ideal stoichiometry in the boundary region while structures shown in Fig. 10(b) and (c) correspond to the surplus of two A atoms and a lack of two A atoms per period, respectively. It is seen that every period of the (830) boundary consists of two groups of units each formed by two units of the (310) and one unit of the (210) boundary. These units correspond topologically to the units shown in Figs 2 and 3. Hence, the structure of the (830) boundary fully conforms to the structural unit model and can be decomposed into the units of the delimiting (210) and (310) boundaries in the same way as in the f.c.c. case. The multiplicity of the type described in detail in Ref. [10] is observed. For example, while the boundary shown in Fig. 10(a) contains (310) units of the type seen in Fig. 2(a), the boundary shown in Fig. 10(c) contains both (310) units of the type seen in Fig. 2(a) and in Fig. 2(b). The multiplicity is, however, further enhanced since topologically identical units differ, in general, compositionally so that (310) and (210) units found in the

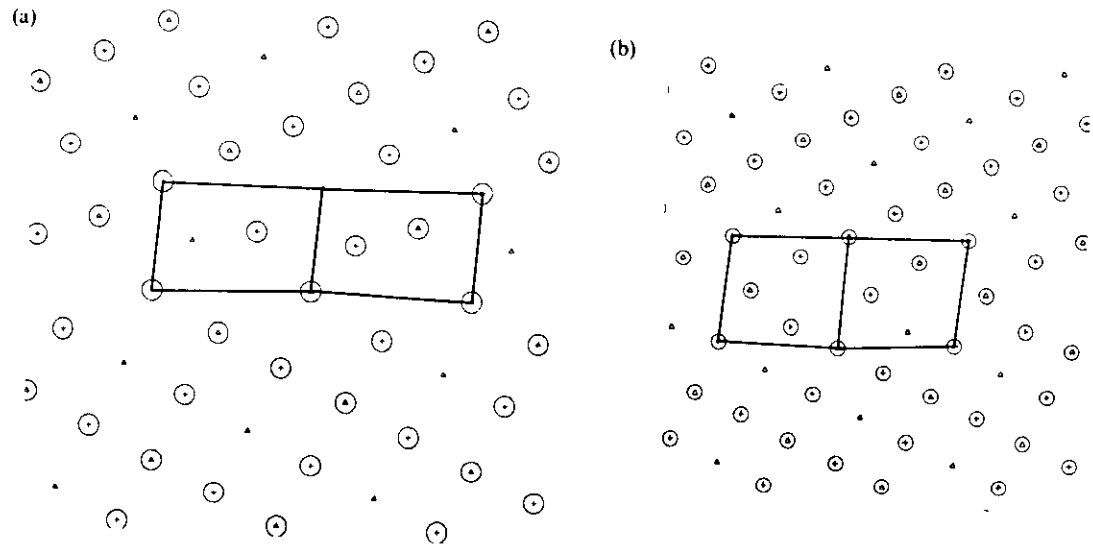

Fig. 8. $\Sigma = 5$ (210) boundary structure in A_3B–$L1_2$ with a surplus of two A atoms per period (a) and four A atoms per period (b) relative to the stoichiometric concentration.

structures shown in Fig. 10 are, in fact, all different. While some of the units are only slightly distorted when compared with those shown in Figs 2 and 3, others are distorted severely and large "holes" are formed in the boundary. As already pointed out in the case of (310) and to a lesser extent (210) boundaries, this appears to be a general feature of stoichiometric boundaries and boundaries in which the deviation from stoichiometry is only small. In addition, calculations of (830) boundaries with larger surpluses of A or B indicated that as the concentration of either A or B in the boundary increased the corresponding structural units became less distorted. This is again the same trend as observed in the case of (210) and (310) boundaries.

The results of the calculations for (830) boundaries conform to the general rules of the structural unit model and structural multiplicity and the distortions of the structural units are of the same type as in the corresponding short period delimiting boundaries. Hence, it is safe to conclude that other long period structures would exhibit the same basic features as does the (830) boundary and the conclusions based on this limited study are likely to be valid for general, low coincidence, long period boundaries.

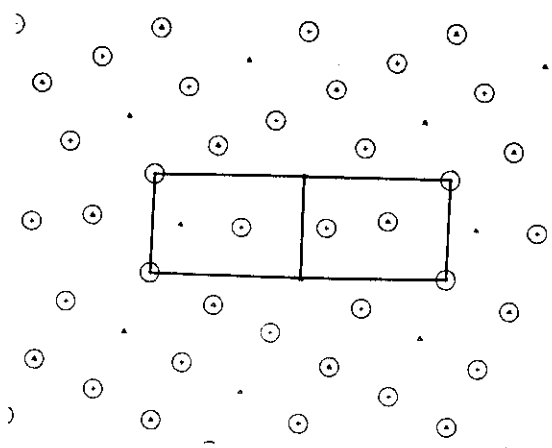

Fig. 9. $\Sigma = 5$ (210) boundary structure in A_3B–$L1_2$ with a lack of two A atoms per period relative to the stoichiometric concentration.

5. DISCUSSION

Two important concepts were established on the basis of the results of atomistic studies of grain boundaries in single component systems [1–6]: the structural unit model which relates the structures of boundaries corresponding to different misorientations [7–9] and structural multiplicity [10–12] which suggests that while boundary structures are not unique they are still composed of well defined structural units. The present calculations dealing with the atomic structure of grain boundaries in A_3B–$L1_2$ compounds, show that both these concepts are also valid in the ordered compounds. However, an extra variability is introduced because of the fact that two kinds of atoms are present. In most cases the atomic structures of grain boundaries in the compound appear to be topologically similar to the structures of the boundaries of the same type in single component f.c.c. materials including the possible multiplicity of structures. The variety of possible structures may differ not only topologically but also compositionally. Consequently, the multiplicity in the alloy system is much more extensive compared to the single component system.

However, the more extensive multiplicity of boundary structures is not the only difference between boundaries in the single component systems and $L1_2$ compounds. The present calculations show that structural units of the boundaries in the $L1_2$ compound are often significantly distorted when

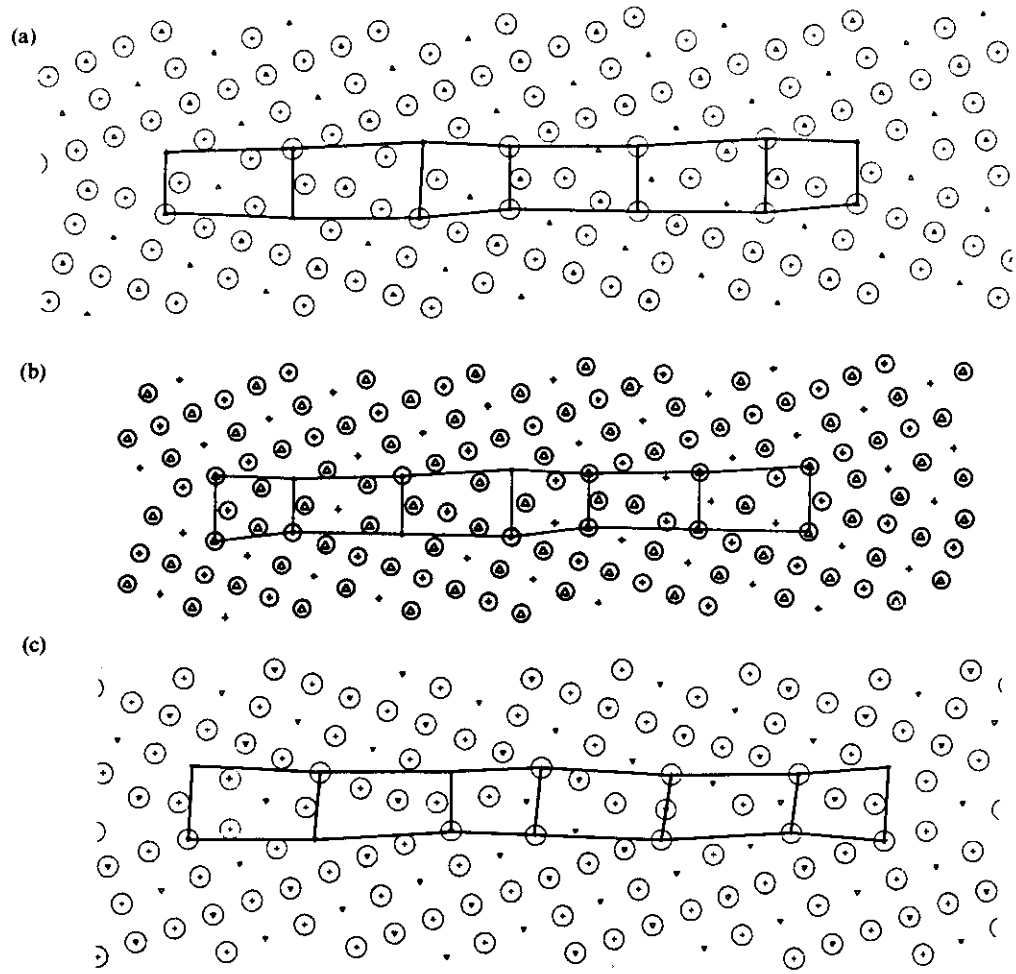

Fig. 10. (a) $\Sigma = 73$ (830) boundary structure in A_3B–$L1_2$ with the stoichiometric composition. (b) $\Sigma = 73$ (830) with a surplus of two A atoms per period. (c) $\Sigma = 73$ (830) with a lack of two A atoms per period.

compared with the corresponding units found in the f.c.c. case. These distortions are particularly large in the case of stoichiometric (310) boundaries and, correspondingly, (830) boundaries which contain (310) units. The physical reason for these distortions is directly related to the ordering tendency. This is described in the present model by a strong preference for formation of nearest neighbour A–B pairs which is evident from the pair-potentials describing the atomic interactions. Comparison of Fig. 4(a) with Fig. 2(b) and Fig. 4(b) with Fig. 2(a) shows that the distortions are of such a type that an almost ideal $L1_2$ lattice is preserved in both the upper and lower grains up to the boundary, so that the above mentioned coordination of the first nearest neighbours is attained as much as possible. Clearly, this would be much disturbed if the undistorted structure of the type shown in Fig. 2 prevailed. The distortions of the stoichiometric (210) boundaries are of the same type, as seen by comparison of Fig. 7(a) with Fig. 3(b) and Fig. 7(b) with Fig. 3(a), but they are appreciably smaller than in the (310) case. The reason is, presumably, that the period of the (210) boundary is shorter which restricts the extent of possible atomic relaxations.

The calculations presented in this paper also show that when deviating away from stoichiometry, either to the surplus of A or surplus of B, the distortions of the structures away from the corresponding structures found in the f.c.c. case, diminish (cf. Figs 5 and 6 with Fig. 2). However, while this is a general trend, in some cases substantial distortions prevail even in non-stoichiometric boundaries [see e.g. one of the units in Figs 5(b) and 6(b)] but they are becoming less frequent as the deviation from stoichiometry increases. Thus it can be calculated that on the average the distortions of the structural units of grain boundaries are the largest at stoichiometric concentration whereas the further the boundary concentration of A and B deviates from the stoichiometric one the more closely the boundary structures resemble the corresponding structures in the single-component system. An exception to this general rule may be some special low Σ short period boundaries, such as $\Sigma = 5$ (210) tilt boundaries, the structure of which will always be only slightly distorted. This trend is entirely consis-

tent with the above explanation of the distortions in stoichiometric boundaries. As the amount of either A or B in the boundary region increases it is obviously less and less possible to form in both upper and lower grains the nearest neighbour environment which is identical to that of the $L1_2$ structure. Furthermore, at sufficiently high concentrations of A or B in the boundary, the boundary region becomes practically composed of only A or B atoms and the boundary structure must become the same as in pure A or B.

Since it is the ordering tendency which appears to determine the principal features of the boundary structures in $L1_2$ compounds it is unlikely that their characteristics are in the framework of central forces strongly affected by details of interatomic interactions. Some important differences might, of course, be expected if directional bonding was dominant but this is unlikely in metallic materials. Indeed, structures calculated in Ref. [34], where many body, embedded atom type [62], interatomic forces were employed, show very similar general features. The reason why structures found in the present study and in Ref. [34] are often different is that in most cases different multiple structures were found in the two studies due to different starting configurations. However, when the same starting configuration was used, such as for the structure shown in Fig. 7(a), the relaxed configurations are practically the same.

In spite of the similarities between A-rich and B-rich boundaries as far as the structural features are concerned, there still exists an important assymmetry when considering segregation of A and B to the boundaries. The reason is that in the framework of the interatomic forces used here a replacement of B by A in the bulk is energetically unfavourable whereas a replacement of A by B in the bulk is energetically favourable. It means that in the bulk it is unfavourable to deviate away from the stoichiometry towards the surplus of A while the opposite is true in the case of surplus of B. Consequently, if there is a surplus of B it might rather stay in the lattice and boundaries would still be practically stoichiometric or possess only a very small surplus of B. On the other hand, if there is a surplus of A it will segregate to the boundaries and A-rich boundaries will be created. It follows than that in A-rich alloys the boundary structure will be similar to that in pure A even at relatively small deviation from stoichiometry in the bulk while in B-rich alloys it will stay more or less the same as in the stoichiometric case, i.e. possessing significant distortions away from the corresponding structures in pure B.

This asymmetry of the grain boundary structures when deviating away from the stoichiometric composition of A_3B compounds may have implications for grain boundary brittleness. It is known that polycrystalline f.c.c. metals or disordered alloys generally do not fail by intergranular fracture. This suggests that grain boundaries for which the structure of which is similar to that of single-component systems are not susceptible to cracking. It can be speculated that boundaries in A-rich $L1_2$ compounds will also be much less likely to break in a brittle manner than in stoichiometric or B-rich compounds since in the former case they will become A-rich and thus relatively undistorted, while in the latter case they will possess stoichiometric, highly distorted structures. This suggests that the most important fact in ductilizing A_3B–$L1_2$ compounds is the deviation from stoichiometry towards A-rich alloys. This is, indeed, in agreement with results of a number of experimental studies. For example, Co_3Ti was found to be ductile when rich in Co but brittle otherwise [22, 24]. Similarly, Ni_3Al and Ni_3Ga could only be made more ductile by addition of boron when these alloys were Ni-rich [24, 26, 53].

The reason why the boundaries possessing distorted structures are more susceptible to brittle fracture may be sought in related changes of electronic structure and cohesion. However, the process of cracking is very complex in metallic materials it either involves competition between bond breaking and dislocation emission (e.g. [54, 55]) or concomitant bond breaking and local irreversible shear deformation at the tip of the propagating microcrack [56–57]. It is likely then that the local resistance to shear and/or to the transmission of slip through grain boundaries, is much higher in the distorted than in the undistorted boundary structures. It has been suggested recently [58, 59, 61] that in Ni_3Al boron attracts nickel and when it segregates to the grain boundaries this attraction enhances the content of Ni in these boundaries. Such an enhancement has been detected using X-ray spectroscopy [61]. It was then suggested that resulting compositional disordering in the boundary region leads to an increase of the mobility of grain boundary dislocations making thus the propagation of the slip through grain boundaries easier [59, 60, 32]. Similarly, if Ni is attracted by boron to grainboundaries, it can be concluded on the basis of the present results that the beneficial effect of boron upon the ductility of Ni_3Al is related to the formation of undistorted structures in Ni-rich boundaries which are then likely to be less resistant to local shear, similarly as boundaries in single component f.c.c. metals. However, for a full understanding of the propensity of grain boundaries to fracture it is necessary to take into account the interplay between the local changes of cohesion and resistance to irreversible shears and, for this purpose, much more detailed calculations are needed.

Acknowledgements—This research is part of the research programme of the Netherlands Foundation for Fundamental Research on Matter (FOM, Utrecht) and has been made possible by financial support from the Netherlands Organization for the Advancement of Pure Research (ZWO, The Hague). This research was also supported by the U.S. Department of Energy, Office of Basic Energy Sciences, Grant no. DE-FG02-85 ER 45129.

REFERENCES

1. R. W. Balluffi, *Metall. Trans.* **13A**, 2069 (1982).
2. A. P. Sutton, *Int. Metals Rev.* **29**, 377 (1984).
3. V. Vitek, in *Dislocations 1984* (edited by P. Veyssiere, L. Kubin and J. Castaing, p. 435. CNRS Press, Paris (1984).
4. P. D. Bristowe and R. W. Balluffi, *J. Physique Paris* **46**, C4–155 (1985).
5. D. M. Duffy and P. W. Tasker, *J. Physique, Paris* **46**, C4–185 (1985).
6. V. Vitek and J. Th. M DeHosson, in *Computer-Based Microscopic Description of the Structure and Properties of Materials* (edited by J. Broughton, W. Krakow and S. T. Pantelides, *Mater. Res. Soc. Symp. Proc.*, Vol. 63, p. 137 (1986).
7. G. H. Bishop and B. Chalmers, *Phil. Mag. A* **24**, 515 (1971).
8. A. P. Sutton and V. Vitek, *Phil. Trans. R. Soc. A* **309**, 1 (1983).
9. D. Schwartz, V. Vitek and A. P. Sutton, *Phil. Mag. A* **51**, 499 (1985).
10. G.-J. Wang, A. P. Sutton and V. Vitek, *Acta metall.* **32**, 1093 (1984).
11. V. Vitek, Y. Minonishi and G.-J. Wang, *J. Physique, Paris* **46**, C4–171 (1985).
12. Y. Oh and V. Vitek, *Acta metall.* **34**, 1941 (1986).
13. G.-J. Wang, D. Schwartz, Y. Oh and V. Vitek, in *Grain Boundary Structure and Related Phenomena*, Trans. Japan Inst. Metals, Vol. 27, 155 (1986).
14. W. Krakow, J. T. Wetzel and D. A. Smith, *Phil. Mag.* **A53**, 739 (1986).
15. R. W. Balluffi, M. Rühle and A. P. Sutton, *Mater. Sci. Engng* **89**, 1 (1987).
16. C. J. McMahon Jr, *Mater. Sci. Engng* **25**, 233 (1976).
17. N. S. Stoloff, in *High-Temperature Ordered Intermetallic Alloys I* (Edited by C. C. Koch, C. T. Liu and N. W. Stoloff, Mater. Res. Soc. Symp., Vol. 39, p. 3 (1985).
18. C. T. Liu and C. L. White, in *High-Temperature Ordered Intermetallic Alloys I* (edited by C. C. Koch, C. T. Liu and N. S. Stoloff), Mater. Res. Soc. Symp., Vol. 39, p. 356 (1985).
19. C. C. Koch, C. T. Liu and N. S. Stoloff (editors) *High-Temperature Ordered Intermetallic Alloys I*, Mater. Res. Soc. Symp., Vol. 39 (1985).
20. N. S. Stoloff, C. C. Koch, C. T. Liu and O. Izumi (editors) *High-Temperature ordered Intermetallic Alloys II*, Mater. Res. Soc. Symp., Vol. 81 (1987).
21. T. Takasugi, O. Izumi and N. Masahashi, *Acta metall.* **33**, 1247, 1259 (1985).
22. T. Takasugi, N. Masahashi and O. Izumi, *Acta metall.* **35**, 381 (1987).
23. T. Takasugi and O. Izumi, *Acta metall.* **34**, 607 (1986).
24. O. Izumi and T. Takasugi, in *High-Temperature Ordered Intermetallic Alloys II* (edited by N. S. Stoloff, C. C. Koch, C. T. Liu and O. Izumi), Mater. Res. Soc. Symp., Vol. 81, p. 173 (1987).
25. K. Aoki and O. Izumi, *Acta metall.* **27**, 807 (1979).
26. C. T. Liu, C. L. White and J. A. Horton, *Acta metall.* **33**, 213 (1985).
27. T. Takasugi and O. Izumi, *Acta metall.* **31**, 1187 (1983).
28. D. Farkas, in *High-Temperature Ordered Intermetallic Alloys I* (edited by C. C. Koch, C. T. Liu and N. S. Stoloff), Mater. Res. Soc. Symp., Vol. 39, p. 133 (1985).
29. D. Farkas and A. Ran, *Physica status solidi* (a) **92**, 973 (1985).
30. D. Farkas, *Scripta metall.* **19**, 467 (1985).
31. D. Farkas and A. Ran, *Physica status Solidi* (a) **93**, 45 (1986).
32. H. J. Frost, *Acta metall.* **35**, 519 (1987).
33. D. Farkas and V. Rangarajan, *Acta metall.* **35**, 353 (1987).
34. S. P. Chen, A. F. Voter and D. J. Srolovitz, *Scripta metall.* **20**, 1389 (1986).
35. S. P. Chen, A. F. Voter and D. J. Srolovitz, in *High Temperature Ordered Intermetallic Alloys II* (edited by N. S. Stoloff, C. C. Koch, C. T. Liu and O. Izumi), Mater. Res. Soc. Symp., Vol. 81, p. 45 (1987).
36. S. M. Foiles, in *High-Temperature Ordered Intermetallic Alloys II* (edited by N. S. Stoloff, C. C. Koch, C. T. Liu and O. Izumi), Mater. Res. Soc. Symp., Vol. 81, p. 51 (1987).
37. W. Kohn, in *Highlights of Condensed-Matter Theory*, p. 1. Soc. Italiana di Fisica, LXXXIX Corso (1985).
38. J. R. Chelikowsky, *Phys. Rev. B* **34**, 5292 (1986).
39. J. K. Lee (editor) *Interatomic Potentials and Crystalline Defects*. T.M.S.-A.I.M.E., Warrendale, Pa (1981).
40. P. D. Bristowe and R. J. Harrison (editors) *Computer Simulation in the Study of Solid–Solid Interfaces*, Surf. Sci. Vol. 144 (1984).
41. M. Yamaguchi, V. Paidar, V. Vitek and D. P. Pope, *Phil. Mag.* **A45**, 867 (1982).
42. V. Paidar, M. Yamaguchi, D. P. Pope and V. Vitek, *Phil. Mag.* **A45**, 883 (1982).
43. G. Tichy, V. Vitek and D. P. Pope, *Phil. Mag.* **A53**, 467 (1986).
44. V. Paidar, D. P. Pope and V. Vitek, *Acta metall.* **32**, 435 (1984).
45. V. Vitek, in *Dislocations and Properties of Real Materials* (edited by M. H. Loretto), p. 30. Inst. of Metals, London (1985).
46. G. Tichy, V. Vitek and D. P. Pope, *Phil. Mag.* **A53**, 485 (1986).
47. P. Beauchamp, P. Veyssiere and J. Douin, *Phil. Mag.* **55**, 565 (1987).
48. J. Th. M. DeHosson, in *Modulated Structures* p. 146. AIP, New York (1979).
49. R. Hultgren *et al.* (editors) *Selected Values of the Thermodynamic Properties of Binary Alloys*. Am. Soc. Metals, Metals Park, Ohio (1973).
50. V. Vitek, A. P. Sutton, D. A. Smith and R. C. Pond, in *Grain Boundary Structure and Kinetics* (edited by R. W. Balluffi), p. 115. Am. Soc. Metals, Metals Park, Ohio (1980).
51. V. Paidar, *Acta metall.* **33**, 1803 (1985).
52. A. G. Crocker and B. A. Faridi, *Acta metall.* **28**, 549 (1980).
53. A. I. Taub, C. L. Briant, S. C. Huang, K.-M. Chang and M. R. Jackson, *Scripta metall.* **20**, 129 (1986).
54. J. R. Rice and R. Thompson, *Phil. Mag.* **29**, 73 (1984).
55. R. Thompson, in *Atomistics of Fracture* (edited by R. M. Latanision and J. R. Pickens), p. 167. Plenum Press, New York (1983).
56. C. J. McMahon and V. Vitek, *Acta metall.* **27**, 507 (1979).
57. M. L. Jokl, V. Vitek and C. J. McMahon, *Acta metall.* **28**, 2479 (1980).
58. E. M. Schulson, T. P. Weihs, I. Baker, H. J. Frost and J. A. Horton, *Acta metall.* **34**, 1395 (1986).
59. E. M. Schulson, I. Baker and H. J. Frost, in *High-Temperature Ordered Intermetallic Alloys II* (edited by N. S. Stoloff, C. C. Koch, C. T. Liu and O. Izumi), Mater. Res. Soc., Vol. 81, p. 145 (1987).
60. P. S. Khodkikar, K. Vedula and B. S. Shabel, *Metall. Trans.* **A18**, 425 (1987).
61. I. Baker, E. M. Schulson and J. A. Michael, *Phil Mag.* (1987). To be published.
62. M. S. Daw and M. I. Baskes, *Phys. Rev.* **B29**, 6443 (1984).